vehicles

MDPI

Article

Lightweight Aluminum–FRP Crash Management System Developed Using a Novel Hybrid Forming Technology

Amir Hajdarevic, Xiangfan Fang *, Saarvesh Jayakumar and Sharath Christy Anand

Institute of Automotive Lightweight Design, University of Siegen, 57076 Siegen, Germany; amir.hajdarevic@uni-siegen.de (A.H.)
* Correspondence: xiangfan.fang@uni-siegen.de

Abstract

The one-step hybrid forming process is a novel process to fabricate a metal fiber-reinforced plastic (FRP) structure with reduced cycle time and cost compared to classical multi-step methods. It is realized by a combined forming tool for both sheet metal and FRP forming to create a hybrid part in only one step. During the forming process, sheet metal pre-coated with an adhesion promoter is joined with the FRP simultaneously. In this work, the crashworthiness and lightweight potential of a hybrid crash management system manufactured with a hybrid forming process were investigated. It includes the experimental behaviors and finite element analysis of glass mat thermoplastics (GMT), as well as aluminum–GMT hybrid structures, under dynamic axial crushing loadings. Beginning with the original geometry of a series aluminum crash management system, the design was optimized for a hybrid forming process, where an aluminum sheet metal part is reinforced by a GMT structure with a ground layer and additional ribs. The forming behavior and fiber filling of the GMT crash box were determined and analyzed as well. Finite element method optimization was used to obtain the optimal geometry of the hybrid crash box with the highest possible specific energy absorption and the utmost homogeneous force level over displacement. A hybrid bumper beam was also developed, along with other necessary connection parts, to join the beam with the crash box and the entire crash management system (CMS) to the vehicle body. The joining technique was determined to be a key factor restricting the lightweight potential of the hybrid CMS.

Keywords: forming of metals and FRPs; axial crushing; crash management system; energy absorption of hybrid structures

Check for updates

Academic Editor: Cheng Lin

Received: 28 October 2025
Revised: 12 December 2025
Accepted: 17 December 2025
Published: 22 December 2025

Copyright: © 2025 by the authors. Licensee MDPI, Basel, Switzerland. This article is an open access article distributed under the terms and conditions of the Creative Commons Attribution (CC BY) license.

1. Introduction

Lightweight design is one of the most important topics in automotive structural development. Fiber-reinforced plastics (FRPs) have demonstrated their lightweight potential for various structural applications [1,2]. Recently, metal–FRP hybrid designs have been increasingly applied [3]. This approach allows for reinforcing metal structures with FRP in highly stressed areas, enabling thinner metal structures and thus leading to vehicle weight reduction.

1.1. Manufacturing of Metal–FRP Hybrid and FRP Structures

Plastics and metals exhibit very different properties such as density, Young's modulus, formability, strength, ductility, and temperature resistance. By combining FRP and metals in a load-bearing hybrid structure, the negative properties of one material may be

compensated by the positive properties of the other. Depending on the level of process integration, the manufacturing of hybrid components can be carried out in one, two, or three stages (see Figure 1). A common and traditional manufacturing process involves producing the plastic and metal components in separate process steps and subsequently joining them in a downstream third process step, for example, bonding, clinching, or riveting [4–7]. This process is referred to as post-molding assembly (PMA). However, aligning the two parts is challenging due to differences in dimensional tolerances. This disadvantage, together with three separate manufacturing steps, leads to increased manufacturing time and costs.

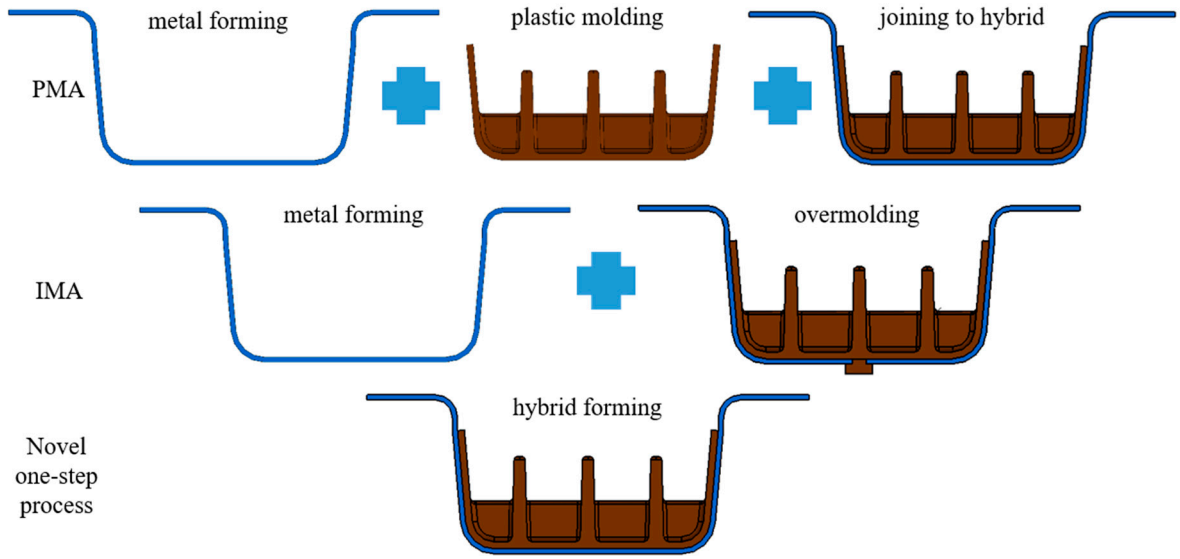


Figure 1. Classification of metal–FRP hybrid structures with respect to number of process steps.

To reduce cycle time and manufacturing steps and avoid the different part tolerances, a preformed sheet metal component can be over-molded by FRPs using methods like injection molding. The creation of a joining could be performed during injection molding, eliminating the need for a separate joining process. This two-stage process is called in-molding assembly (IMA) [8–11].

To further reduce the processing costs of IMAs, several researchers have investigated the forming of thin metal sheets using the pressure of molten plastics in an injection molding process [12–14]. Wehmeyer [15] demonstrated a medium-based forming of 1.0 mm thick, soft deep-drawing steel DC04 with a polypropylene (PP)-based plastic melt. In ref. [16], an injection molding machine was equipped with a blank holder function to control the sheet metal flow during the manufacturing of the hybrid cylindrical cup geometry. By closing the mold, the metal sheet was initially deep drawn, and once the mold was fully closed, the sheet was further formed by the pressure of the plastic melt. However, such processes were only feasible for very simple rotationally symmetrical parts made from mild steels. For high-strength steels, or even advanced high-strength steels, as well as for complex geometry, this process has not been implemented.

Additionally, the mechanical properties of injection-molded FRPs are limited due to significant fiber damage occurring during the manufacturing process. Shear-induced fiber breakage leads to reduced fiber lengths to well below 1 mm, which in turn decreases both the stiffness and the strength of the FRP [17]. In contrast, higher fiber length and consequently improved properties of the final components can be achieved through compression molding [18–20]. Here, thermoplastics with longer fibers (up to 10 mm) are press-formed in a well-sealed die to produce the final part. This type of material is classified as a long-fiber

thermoplastic (LFT). Furthermore, glass mat thermoplastic (GMT) materials with significantly longer fiber lengths can also be processed with compression molding. To further reinforce GMT materials, woven-fabric layers can be added to this material. This kind of material is named GMTex, which is provided by the company Mitsubishi Chemical Advanced Materials Composites AG, Schaffhausen, Switzerland.

Based on the results in refs. [15,16] and the mechanical benefits of compression-molded FRPs with long fiber lengths [20], Fang and Kloska [21] developed a new one-step hybrid forming process for the simultaneous forming of sheet metals and FRPs. In hybrid forming, the forming of the sheet metal component, the forming of the FRP, and the joining process are realized simultaneously in a single tool in one process step. The FRP is joined to sheet metal over the entire part surface by adhesive bonding, enabled by an adhesion promotor (such as VESTAMELT from Evonik), which is precoated to the sheet metal. FRP can have different thicknesses and rib structures to reinforce the sheet metal components effectively.

In hybrid forming, sheet metal must be preheated (200 °C) to activate the adhesion promotor and then placed into a press tool along with a molten LFT/GMT extrudate. The hybrid press tool setup corresponds to a sheet metal forming die, consisting of a die, a punch, and a blank holder. A crucial factor for the hybrid forming process is tool sealing. As the forming of metal sheets is partially performed by the hydrostatic pressure of the LFT/GMT on the cavity side, any leaks in the tool will result in press-out of LFT/GMT, accompanied by a pressure loss and hence an insufficient forming of the sheet metal. In ref. [21], various tool and sealing concepts were developed for both a closed tube geometry and an open U-profile. These concepts were expanded in ref. [22] for a completely open-end component with a simplified die sealing concept. The new die concept also allows plastic-free areas at the flanges, allowing more design freedom for hybrid parts, such as welding of the steel–FRP hybrid components to steel parts. With minor adaptations, most of the geometries used in vehicle structures can be covered with these die concepts.

The final hybrid-formed component is a combination of thinner sheet metal and a load-optimized FRP rib structure acting and complementing each other in producing a lightweight component. For example, a hybrid control arm made of PA6-GF40 and 2 mm thick high-strength DP800 steel (tensile strength > 800 MPa) has been developed and successfully formed, demonstrating a weight reduction of 20% compared to a serial component made of thicker DP800 steel [22,23].

At present, FRPs processed in hybrid forming are usually based on polyamide 6 (PA6) or PP with long glass fibers, as these materials offer a good compromise between good processing properties and acceptable costs. In addition to LFTs, whose fiber lengths in the final component are limited to a maximum of 10 mm, GMTs have become established as a material in recent years, particularly for crash-relevant structural applications [24,25]. GMT is almost exclusively used with PP as the matrix material. The material consists of glass fiber mats with fiber lengths of 20–50 mm, impregnated with thermoplastic melt and consolidated by press pressure. GMT composites offer a high strength-to-weight ratio and excellent energy absorption capabilities [26]. Moreover, it is also possible to integrate continuous fiber fabric layers into the hybrid forming process (e.g., GMTex) to significantly improve the mechanical properties [27].

Although significant progress has been made in lightweight multi-material structures, there remains a clear research gap in forming-integrated aluminum–FRP hybrid components that combine structural performance with manufacturing efficiency. Current industrial solutions rely on sequential forming and joining steps, such as PMA and IMA mentioned above, which increase cycle time and tooling cost, while limiting geometric

freedom and energy absorption stability. In addition, the crash behavior of GMTex hybrid structures at component level should be systematically investigated, extending the knowledge about LFT materials. The motivation is driven by industrial demand for lightweight and crash-robust front-end structures, as well as the need for hybrid design concepts that enable high energy absorption in combination with structural integrity. Therefore, this study aims to close these gaps by evaluating a one-step hybrid forming technology and assessing its feasibility for crash management systems through combined experimental and numerical analysis.

1.2. Finite Element Modeling

The finite element method (FEM) is the prerequisite for the introduction of new materials and manufacturing processes in the automotive industry. It plays an essential role in predicting structural behavior and realizing lightweight design potential.

Many FEM optimizations on FRP with different architectures have been conducted. In refs. [28,29], comprehensive overviews of multi-material crash absorbers and their modeling can be found. Among them, Reuter and Tröster [30] recently developed a lightweight FRP–metal hybrid structure using finite element methods and compared its performance with pure aluminum and pure FRP tubes. These FRP–metal hybrid structures could produce 37% higher specific energy absorption compared to pure aluminum tubes. Lu et al. [31] conducted a detailed study of the energy absorption performance in CFRP/aluminum hybrid square tubes with varying thicknesses.

Since the hybrid structures involve many design variables and parameters for design optimization, the computation time and effort through manual iterations in refs. [30,31] were enormous. In contrast to the manual approach, the topology optimization process significantly minimizes the time and effort. Teimouri et al. [32] and Y. Li et al. [33] conducted a topology optimization for hybrid structures and achieved drastic mass reduction from solid structures. Kloska and Fang [23] developed a design and optimization methodology for linear-static load cases through a topology optimization with the FEM solver Optistruct. The methodology makes it possible to determine the lightweight construction potential by reducing the sheet thickness of existing metal components and, at the same time, to obtain a design proposal for the FRP rib structure.

For many vehicle structure developments, a design with static load cases alone is not sufficient. Especially for crash structures, plasticity, damage, and failure of metal, FRP, and adhesive must also be considered. The above-mentioned topology optimization cannot currently be applied to dynamic load cases due to the continuously changing stress states in the parts [34].

Existing material models for FRP materials face substantial challenges due to the highly anisotropic characteristics of these materials—particularly regarding plasticity, damage, and fracture [35]. Many models have been implemented in solvers, such as LS-DYNA, RADIOS, and PAM-Crash. Based on the specific degradation laws used in LS-DYNA, the models are primarily categorized into progressive failure (MAT 22 and MAT 54) and continuum damage mechanics models (MAT 261 and MAT 262) that are preferentially developed for FRPs with endless fibers.

To predict the performance of GMT materials incorporated with endless fibers, Hörmann and Wacker [36] and Feraboli et al. [37] proposed and validated the usage of the progressive failure model MAT 54 in LS-DYNA. This model could make reasonable predictions by using limited material data [36,37]. Therefore, the MAT 54 model was preferred in this work over the continuum mechanics approach, which required extensive material data.

The performance of FRP–metal hybrid structures is strongly influenced by adhesive behavior [38]. Finite element modeling of adhesives is primarily categorized into continuum mechanics and cohesive zone modeling. Continuum damage mechanics models require excessive computational time. Therefore, the cohesive zone technique delivering robust predictions within a cost-effective computational timeframe is often used [39]. A cohesive zone model is formulated using traction-separation relationships for individual loading modes (mode I and mode II) or combined loading, the so-called mixed mode. The state of stress is defined via a direct relationship to the displacements in the three local stress directions of the element, with one direction describing the peel deformation and the other two describing the shear deformation.

MAT 138 and MAT 186 are the simplest versions of cohesive zone models in LS-DYNA. Both these models, however, lack the strain rate dependency effects in traction-separation relationships. Therefore, the MAT 240 model was developed, which includes the strain rate dependency of yield stresses and energy release rates in different modes, respectively.

Jayakumar et al. [38] proposed an FEM process chain to model a hybrid structure consisting of GMT and aluminum (Al) during crash simulation by taking all these aspects into account. In this process, three materials models of LS-DYNA were combined: the progressive failure material model MAT 54 was applied on LFT, MAT 24 on metal, and the cohesive zone model MAT 240 on the bonding layer between steel and LFT.

1.3. Target and Structure of the Work

Based on the advantages of the novel one-step hybrid forming process for metal and FRP, the objective of this work is to develop, validate, and manufacture lightweight aluminum–GMT structures for energy-absorbing applications using GMTex materials with enhanced elastic modulus and strength compared to LFT. The new CMS should reduce the weight of the original full Al-CMS or increase its mechanical performance or improve both. The appropriate rib structures of GMTex for the crash box should be found using FEM and confirmed by experiments. The force–displacement characteristics, energy-absorbing ability, and deformation and failure behaviors of crash box profiles of both pure GMTex and GMTex–Al hybrid should be investigated and compared experimentally and through the FEM. To demonstrate the feasibility of the hybrid concept for a body structure assembly, a new crash management system (CMS)/bumper system for passenger vehicles should be designed and developed. This CMS should meet the major mechanical requirements on bumper systems of a passenger vehicle, such as the low-speed RCAR 10° bumper structure test, the RCAR bumper compatibility tests, and the tow hook tests.

This paper is structurally divided into the following sections: After the introduction in Section 1, Section 2 will present the work methodology, starting with material selection and characterization, introduction of hybrid forming tool concept and process setups, benchmarking of the CMS, and finally the finite element models for the CMS. In Section 3, the results of material characterization are presented and discussed. Section 4 presents the development of the most essential part of the CMS for energy absorption, the crash box. The design and optimization of the pure GMT crash box is first shown, with all the details, and compared to the hybrid crash box. Both FE simulations and dynamic tests using drop weight tower tests are discussed. Finally, Section 5 presents the development and optimization steps of the aluminum–FRP cross-member as well as the simulation results of the RCAR low-speed structural test of the entire CMS, followed by the conclusions and outlooks in Section 6.

2. Methods

The methods presented in this section address several key aspects, including material selection and characterization, benchmarking and target setting for the new hybrid CMS, specification of hybrid forming tools, as well as the experimental and finite element setups for the CMS.

2.1. Material Selection

In this study, two typical aluminum alloys used in the automotive industry were investigated. The materials were supplied by Speira GmbH, Bonn, Germany. A 1.5 mm AA5182 alloy was selected for the crash box based on its good formability. For the cross-member, a 1.5 mm heat-treatable AA6451 alloy was selected to achieve high bending strength. In both cases, glass mat thermoplastic (GMTex X121), provided by Mitsubishi Chemical Advanced Materials Composites AG, was used as reinforcement in addition to the Al alloys. GMTex X121 is a GMT material with a fiber volume fraction of 40%, provided by Mitsubishi. The glass fibers in this material consist of 46 vol % discontinuous fibers and 54% continuous fibers (plain-woven layers). The continuous woven layer is composed of 80% fibers oriented in the longitudinal direction (warp) and 20% fibers in the transverse direction (weave). The GMTex material has significantly higher specific strength and tensile modulus compared to LFT materials. This material exhibits a very homogeneous glass fiber distribution and is therefore commonly used for crash-relevant components, according to Mitsubishi.

To further improve the stiffness and strength of the CMS bumper beam, a unidirectional (UD) tape (GF-PP-61-51-260) with a fiber volume content of 61% was also utilized in addition to GMTex.

Hybrid components consisting of Al and GMTex were bonded together with the help of bonding agent VESTAMELT, provided by Evonik Operations GmbH, Marl, Germany. A bonding thickness of approx. 100 µm is recommended and applied on aluminum sheets by a powder coating process. To generate a firmly bonded connection between aluminum and GMT, the precoated aluminum sheets were preheated to a temperature between 190 and 200 °C.

2.2. Material Characterization

Since detailed material data are indispensable for the FEM material model, material tests were conducted as follows.

To characterize the yield and hardening behaviors of AA5182 and AA6451, uniaxial tensile tests were performed on small, smooth dog-bone (SDB) specimens. Each SDB specimen had a section length of 20 mm. The tests were conducted according to DIN EN ISO 6892-1 [40] at low strain rates (machine speed = 2 mm/min) using a 100 kN universal tensile testing machine Z100 (ZwickRoell GmbH & Co. KG, Ulm, Germany). The force was measured using the load cell of the machine. The strain was measured using the digital image correlation (DIC) method with ARAMIS Professional 2018 software from GOM. For the tensile tests, two GOM ARAMIS 5M CCD cameras with a maximum frame rate of 29 Hz and a maximum resolution of 2448 × 2050 pixels were used. The frame rate was set to 1 Hz, the facet size to 12 pixels, and the point distance to 6 pixels. The same technique was applied to the GMTex material.

For testing of GMTex material, the specimens first had to be made using a compression molding tool, as the material properties are highly dependent on the "forming" conditions and the lay-up of GMTs [38]. In ref. [38], it was found that GMTex material in a multi-layer configuration shows a much higher Young's modulus and strength. In a real component, several layers of GMT must be stacked in the tool to achieve the desired material distribution

in the part through compression molding. A single layer is usually too thin. Thus, in this work, two plies of the GMTex material were heated to 200 °C, manually placed on the heated tool, and pressed to form a U-profile, as shown in Figure 2a,b. The press parameters are given in Table 1. As a reference, the unpressed GMTex was also tested, as shown in Figure 2c. Due to the size of the U-profile, it was not feasible to prepare standardized ISO 527-4 [41] specimens. Therefore, smaller specimens with dimensions of 110 × 10 × 4 mm^3 were used to characterize the tensile behavior of both the unpressed and the pressed GMTex samples (see Figure 2b).

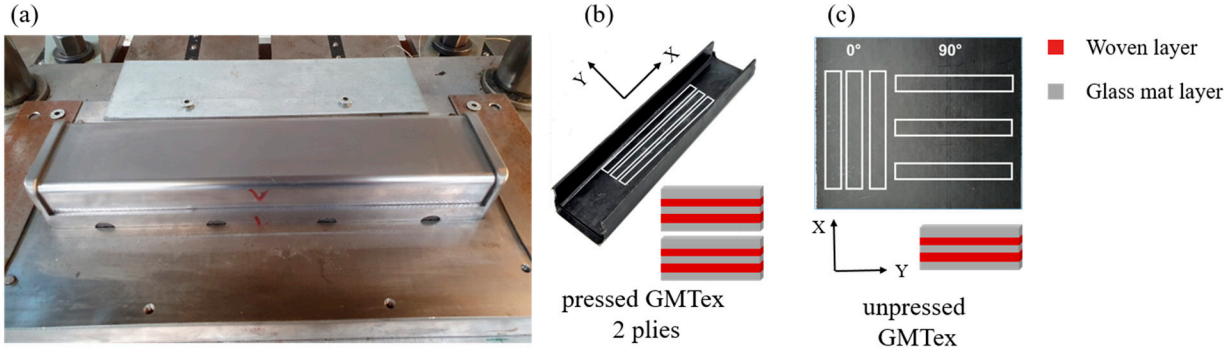


Figure 2. (**a**) Press tool for manufacturing multiple-ply pressed GMT components, (**b**) specimen location from pressed hat profiles, and (**c**) from the extrudate.

Table 1. Process parameters.

Wickert Press WKP 2000 S Parameter	Value
Pressing force [kN]	600
Die velocity [mm/s]	5
Holding time [s]	30
Tool temperature [°C]	80

The compression tests on GMTex were conducted using a combined loading compression (CLC) fixture in accordance with ASTM D6641 [42], employing the same testing procedure and specimen geometry as used for the tensile tests.

The bonding agent was characterized using lap shear and cross-tension specimens as described in ref. [21]. The specimen dimensions are shown in Figure 3. A common lap shear test specimen, based on DIN EN ISO 1465 [43], with a standardized overlap length of 12.5 mm and a small width adjustment, was selected.

The cross-tension specimen was newly developed, as described in ref. [21]. By using an interchangeable tool insert, lap shear and cross-tension specimens can be produced with the same pressing tool. To prepare the lap shear and cross-tension specimens, the 1.5 mm thick aluminum sheet needed to be preheated to approximately 200 °C (bonding agent activation temperature) before manual transfer into the press tool. Pre-weighed GMT was then placed into the tool and pressed at 250 bar so that the GMT material flowed over the bonding agent to achieve adhesive bonding. Details about the tools used are thoroughly described in ref. [44]. The dimensions of the cut GMTex piece for both specimens were 50 × 100 × 4.5 mm^3. The bonding area for the lap shear tension specimen was 625 mm^2, and for the cross-tension specimen, 225 mm^2. All lap shear tests were carried out using an Ibertest TESTCOM 50 tensile testing machine (Ibertest S.A., Madrid, Spain). A clip-on extensometer with a gauge length of 50 mm was used to evaluate the strain.

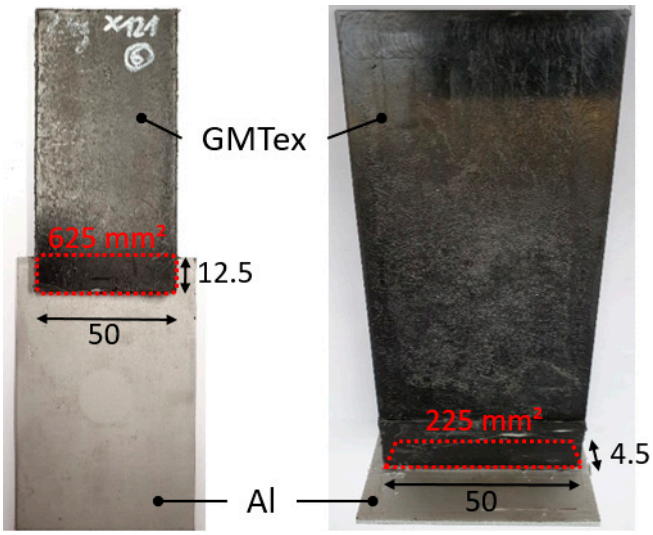


Figure 3. Shear and cross-tension specimens with bonding areas.

2.3. Hydraulic Press and Forming Tool Concept

For compression molding of the test specimens and, later, for the hybrid forming of CMS components, a Wickert WKP 2000S hydraulic press (WICKERT Maschinenbau GmbH, Landau in der Pfalz, Germany) with a maximum press force of 220 t was used. As mentioned in ref. [21], the press technology required for hybrid forming is almost identical to that used for metal forming and compression molding. Vertical-closing hydraulic or servo-mechanical presses, having a hold function at the bottom dead point, are necessary for this process. Key aspects of metal forming include forming speed and the control of blank holder forces. This can be achieved either through an actuation system integrated into the bolster plate of the hydraulic press (hydraulic die cushion) or by using gas pressure springs in the tool. Due to the lateral forces that occur during compression molding and hybrid forming, the press should feature a highly rigid side-guidance system.

To produce Al–GMTex hybrid structures in this work, the tool concept developed by Fang and Kloska [21,22] for hybrid forming of a U-profile was utilized. This concept allows the manufacturing of open hybrid components and can be adapted for various sheet metal thicknesses. The configuration of the hybrid press tool used in this study is shown in Figure 4. The complex GMTex rib structure, acting as a negative contour, is integrated into the punch. The blank holder is placed over the die cushion of the press and is significantly thicker compared to conventional deep-drawing tools to create space for the GMTex material to be placed in the die cavity between the punch and blank holder when the blank holder is moved to the upper position. A major technical challenge is ensuring complete tool sealing, as the sheet metal is partially formed by the hydrostatic pressure of the molten GMTex. Any leakage results in pressure loss, insufficient sheet metal forming, and incomplete rib filling. Therefore, the tool incorporates dedicated sealing surfaces and a controlled blank holder system. The blank holder (force) serves two key functions: sealing the GMTex from press-out, and controlling the flow of the sheet metal. Initially, the blank holder, which is mounted on the die cushions and positioned above the punch, creates a free volume for the GMTex. As the upper tool closes, it moves the blank holder against the die cushions while the punch forms the sheet metal and molten GMT simultaneously in a single process step. The tool is heated to 90 °C using electric heating cartridges to ensure proper processing conditions.

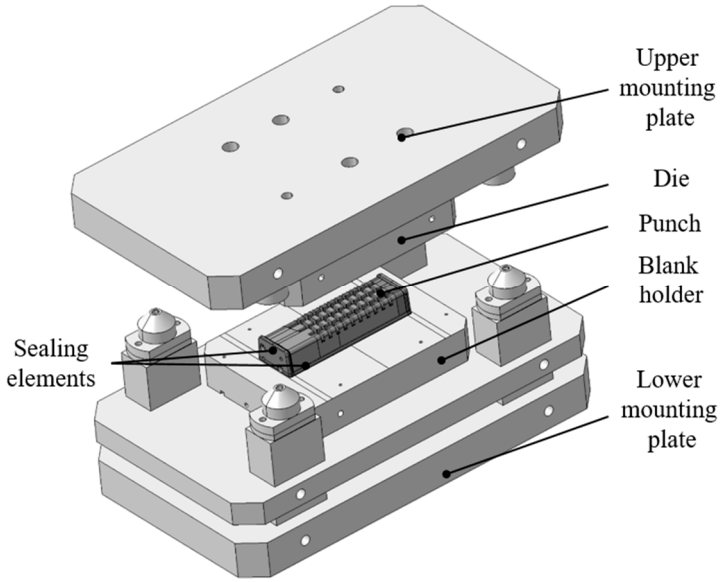


Figure 4. Tool concept for the manufacturing of open hybrid parts.

2.4. Drop Tower Test

To determine the deformation and failure behavior of GMTex and Al–GMTex hybrid structures under high-speed loading conditions and to validate the FE model, dynamic crushing tests were performed using a drop tower equipped with a guided impactor consisting of a rigid steel mass with a flat loading surface, guided by low-friction linear bearings to prevent lateral deviation. A precise alignment with the longitudinal axis of the crash box was thus ensured. To ensure good repeatability, the lower end of the crash-box specimens was mounted in a rigid fixture with a clamping length of 50 mm, preventing rotations and lateral movements while allowing only axial deformation.

The applied energy for pure GMTex components was about 3 kJ, with a falling mass of 200 kg and a falling height of 1.5 m. The GMTex–Al hybrid crash box was crushed at a velocity of 6.2 m/s with a falling mass of 370 kg and a falling height of 1.9 m, yielding a kinetic energy of 7 kJ. The time-dependent force and displacement of the impactor during the tests were measured using load cells and a laser tracking system, respectively. Additionally, the crushing of pure GMTex components and the folding progression of the hybrid components were recorded with a high-speed camera system (5000 frames/s) for monitoring the deformation behavior of the structures.

2.5. Benchmarking and Target Setting

To develop a new Al–FRP hybrid CMS, a reference CMS must be defined, and its performance must be determined. In this work, the front CMS of the current Ford Focus was chosen. The reference CMS is made of extruded aluminum and is shown in Figure 5a. It has a total weight of 4.2 kg, consisting of a cross-member, crash boxes, and a connector plate. According to [3], the bumper CMS must meet both high-speed and low-speed crash test requirements. For a high-speed crash, such as ECE R94 or the Euro-NCAP crash, a full-vehicle test is required, which was not possible in this work. For low-speed crash conditions, tests like the RCAR 10° test and the RCAR bumper compatibility test at the component level may be applied.

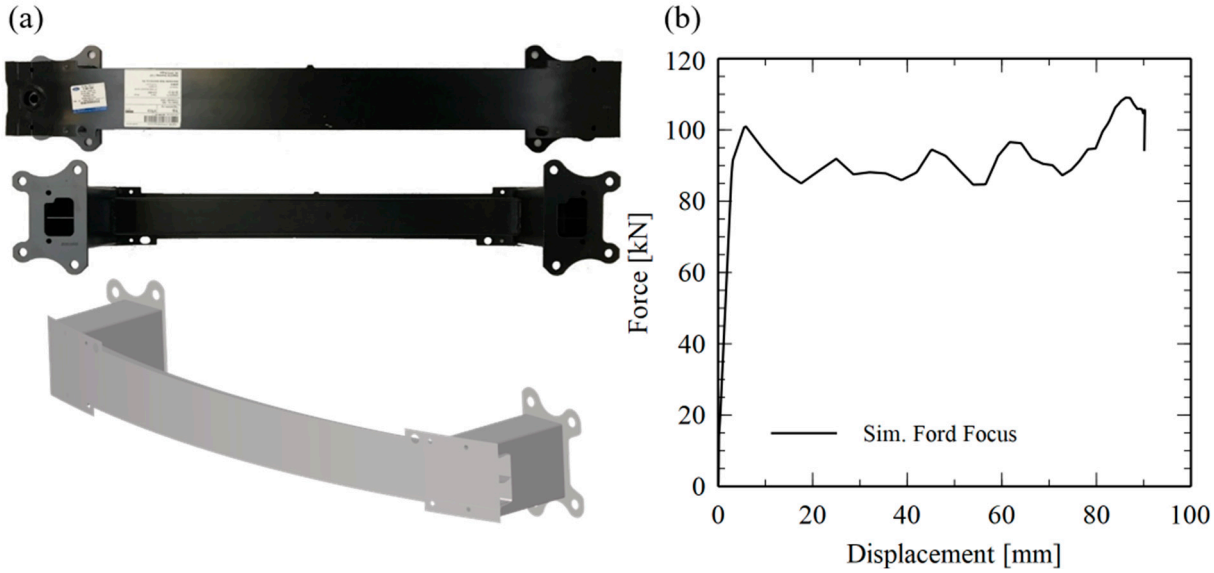


Figure 5. (**a**) Reference CMS, photo, and reverse-engineered CAD picture; (**b**) force–intrusion curve.

In the RCAR bumper compatibility test, the bumper must be impacted with 10 ± 0.5 km/h impact speed against a deformable barrier with an overlap of 100% [3]. This test requires a minimum bumper overlap with the barrier in the Z direction of 75 mm. For minimum damage and minimum repair cost during RCAR tests, the bumper beam must provide high structural stiffness and low deflection.

During the RCAR 10° low-speed structural crash test, the bumper of a car is to be impacted against a fixed and rigid barrier, aligned 10° to the vehicle velocity direction, with 40% overlap [3]. The test speed is 15 ± 1 km/h. The requirement is that a certain level of force must not be exceeded to protect the front body structure (such as front rails) from plastic deformation. Additionally, car components, such as the front cooling device or a front lamp, must not be damaged to reduce repair costs. Therefore, in addition to the force level, max. displacement must also be limited.

To determine the reference low-speed crash performance, small samples were cut from a reference bumper CMS, and their material properties were measured as given in Table 2. The whole bumper was digitized, and CAD data were created by reverse engineering, as shown in Figure 5a. With these CAD and material data, a model was built using FEM at the component level with a rigid slide, as described in ref. [3]. The force–displacement curve of the RCAR 10° low-speed structural test is shown in Figure 5b. It served as the target for the new hybrid CMS.

Table 2. Tensile properties of the reference crash box and cross-member alloy.

Material	Temperature [°C]	$R_{p0.2}$ [MPa]	R_m [MPa]	A_{15} [%]
Al crash box	RT	110	230	17
Al cross-member	RT	160	350	18

2.6. Finite Element Models

Figure 6 shows the FEM model setup for the GMT and hybrid crash boxes developed in this work. The impactor was modeled as a rigid body. Automatic single-surface contact was employed between the crash box and impactor as a global contact for both crash boxes. Automatic surface-to-surface contact between the layers and ribs, and between the ribs themselves, was employed for both crash boxes. The lower portions of

both crash boxes were fixed in all degrees of freedom, similar to the real drop tower tests mentioned above.

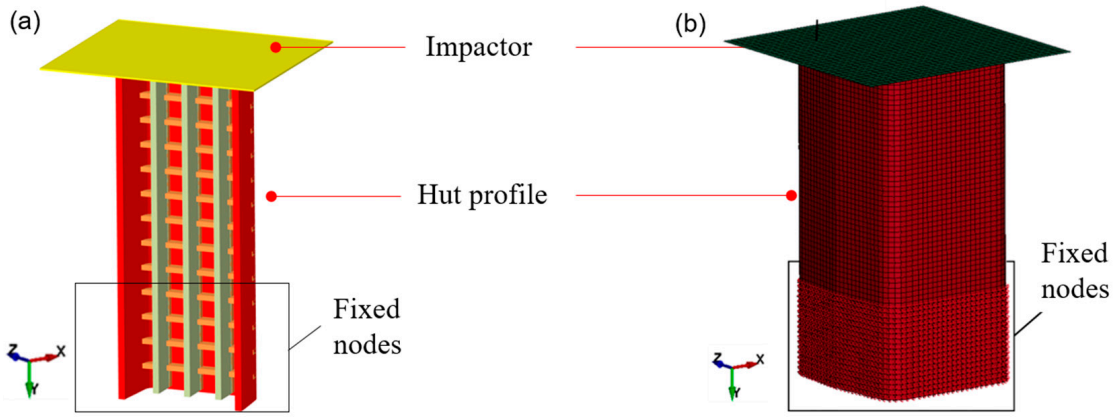


Figure 6. FEM model setup of (**a**) GMT and (**b**) Al–GMT hybrid crash boxes.

Figure 7 shows the FEM model setup of the hybrid CMS for the RCAR 10° low-speed structural test. The CMS was impacted with 40% overlap, and the velocity was 15.6 km/h. The CMS was affixed to a mass element representing the car's mass, which weighed 995 kg and was positioned at the mass point (MP). A contact algorithm similar to the one employed for the hybrid crash box above was incorporated into the Al–GMT hybrid CMS. Thin shells were used to model the GMT materials, with fully integrated elements of type 16 and an element size of 3 mm. For the hybrid profiles (similar to those in Figure 6), two thin shells (for Al and GMTex) were stacked together and connected by cohesive zone elements.

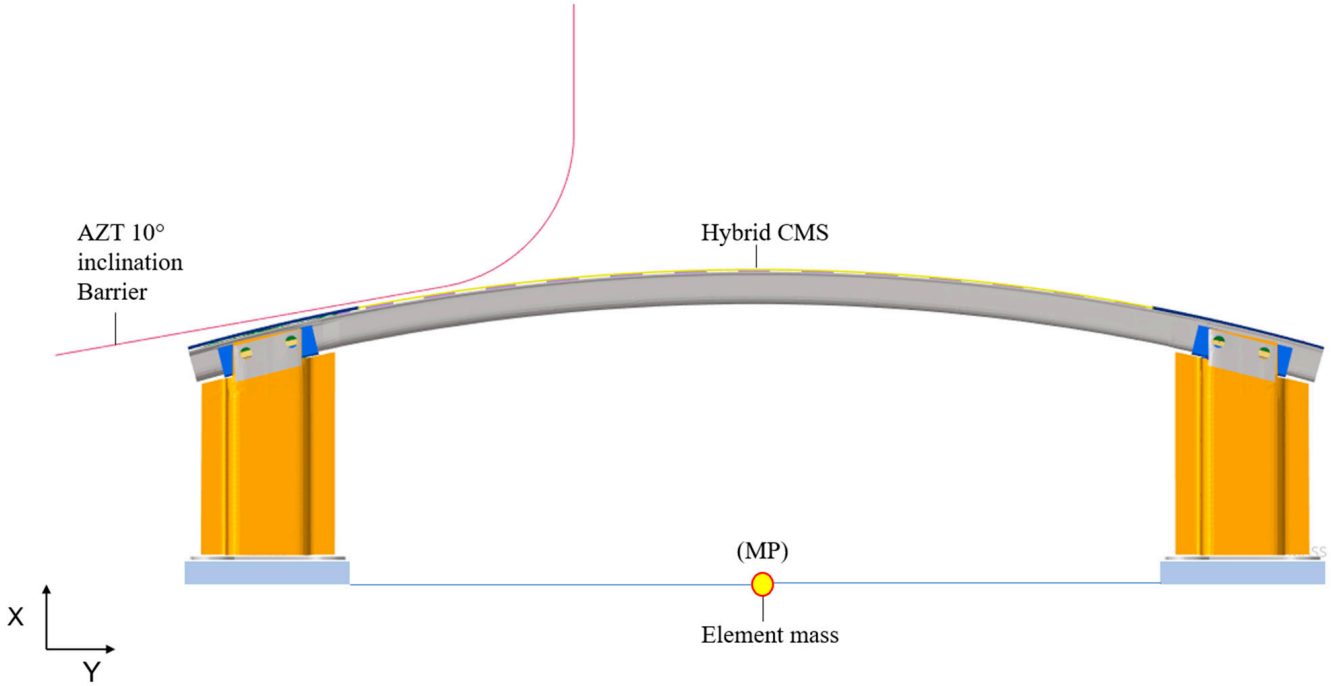


Figure 7. FEM model setup of Al–GMT hybrid CMS for the RCAR 10° load case.

As introduced in Section 1.1, the FE methodology developed in ref. [38] for the design of hybrid structures under crash loading consists of the following material models: MAT 54 for modeling the GMT material, CZM MAT 240 for modeling the adhesive, and MAT 24 for modeling aluminum. This methodology was used for the design of hybrid structures in this

work. The MAT 24 linear-isotropic plasticity model is widely recognized for its effectiveness in simulating the behavior of metallic materials. In this study, material characterization was conducted for the aluminum alloys, and the resulting stress–strain curve was incorporated into the MAT 24 model.

To model the behavior of the GMTex material in simulations of hybrid structures, MAT 54 with a failure model was chosen. As in any other anisotropic material model, MAT 54 requires the following material data; tensile strength in longitudinal (Xt) and transverse directions (Yt), compressive strength in longitudinal (Xc) and transverse direction (Yc), and shear strength (Sc). These values were obtained from material testing, as discussed in Section 3 Material anisotropy through fiber orientation was defined using the AOPT option in conjunction with the vector description (v1, v2, v3) in MAT 54. This option defines a local material axis for each finite element of the plastic part. One of the reasons MAT 54 was considered for this work was its underlying failure criterion. In the post-elastic region, MAT 54 employs the Chang–Chang failure criterion to model damage. The Chang–Chang criterion is governed by four failure modes: fiber tension, fiber compression, matrix tension, and matrix compression. The values of these failure modes are tracked throughout the simulation. As long as the values remain less than one, there is no failure of the elements. When any of the four modes reach a value of one or greater, damage within the particular element is initiated, resulting in stiffness degradation and eventual deletion. Detailed information about the constitutive relations and governing equations of MAT 54 can be found in ref. [38].

For the calibration of the MAT 54 parameters, the tensile and compressive properties obtained from the specimen tests were entered directly into the MAT 54 material card. Instead of performing a separate analytical curve fitting using the stress–strain curves of GMTex material on specimens, the calibration was carried out through component-level validation. Specifically, the crushing behavior of the GMTex crash box was simulated and compared with experimental results. The close agreement between simulation and experiment confirmed that the MAT parameters accurately reproduced the material behavior at the component level.

Since metal and FRP are joined together using the bonding agent VESTAMELT in this work, the material behavior of bonding agent in the simulation was modeled using MAT 240 with the CZM modeling technique. This technique helps model the interlaminar failure of adhesives. As discussed in Section 2.2, the VESTAMELT bonding agent was characterized using the lap shear and cross-tension tests. These tests serve as the basis for MAT 240 development from which the tensile and shear strengths were obtained. The parameter calibration was carried out using the software LS-OPT 6.0. Using LS-OPT, the MAT 240 parameters were iteratively adjusted until the simulated force–displacement curves matched the experimental results, as shown in Section 3. This procedure resulted in calibrated energy release rates for the MAT 240 model.

Figure 8 summarizes the complete methodological workflow of this study, covering all major stages from material characterization and material model calibration to crash box optimization, component manufacturing using hybrid forming, experimental validation, and finally the integration of all processes into the hybrid crash management system.

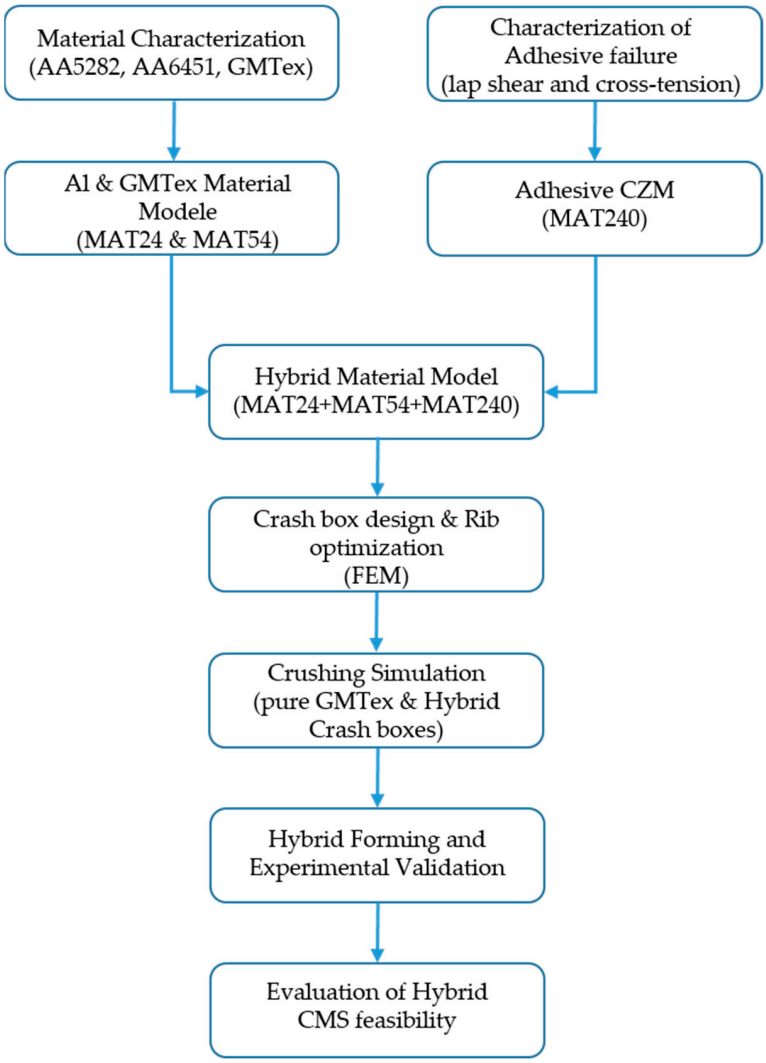


Figure 8. Methodological workflow of the study.

3. Material Test Results for CMS Development

Tensile tests, as described in Section 2.2, were conducted. For each material, three tests were performed, and the results are shown in Figure 9. A gauge length of 15 mm was used to evaluate the strain. Table 3 lists the measured mean values and standard deviations of the mechanical properties of AA5182 and AA6451.

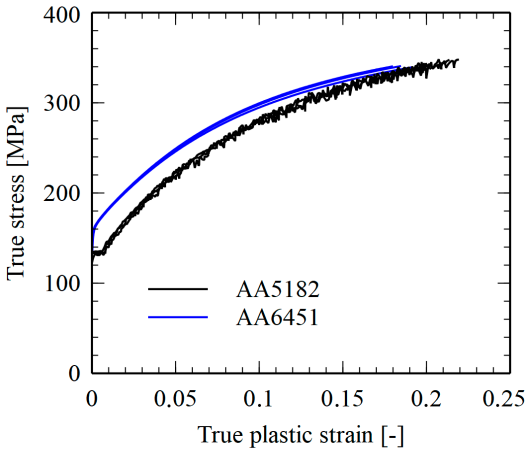


Figure 9. Flow curves of AA5182 and AA6451 at quasi-static and RT conditions.

Table 3. Tensile properties of AA5182 and AA6451, presented as mean values with corresponding standard deviation.

Material	Temperature [°C]	$R_{p0.2}$ [MPa]	R_m [MPa]	A_{15} [%]
AA5182 H111/O	RT	132.3 ± 0.4	284.4 ± 0.5	30 ± 0.6
AA6451 T4	RT	161.5 ± 3.1	281.6 ± 2.0	30.9 ± 0.3

The stress–strain curves of the GMTex material under tensile and compressive tests were reproducible as well. The three measured stress–strain curves for each material are shown in Figure 10.

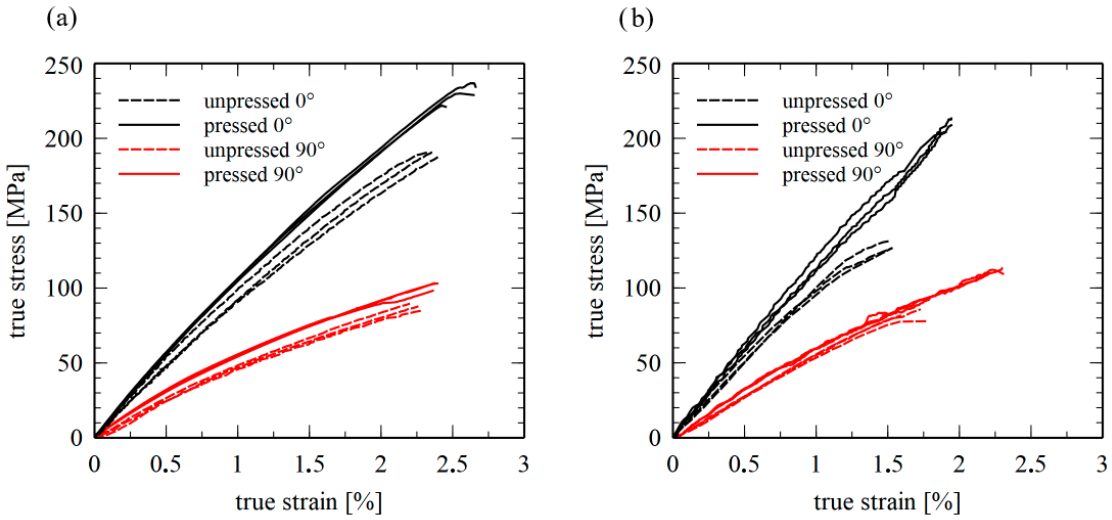


Figure 10. Stress–strain curves of unpressed and pressed GMTex material: (**a**) tensile and (**b**) compressive tests.

Figure 10a shows the stress–strain curves of unpressed and two-ply pressed GMTex material (as described in Section 2.2) in the longitudinal direction. The two-ply pressed GMTex had significantly higher stiffness and strength compared to the unpressed material. The tensile strength in the longitudinal direction increased by approx. 20%, and the compressive strength increased by about 40% for the pressed material. Similarly, the tensile and compressive properties of GMTex in the transversal direction are shown in Figure 10b. As expected, the tensile and compressive strengths in the transversal direction were significantly lower than those in the longitudinal direction. Again, there was a clear difference between the pressed and unpressed material. The material properties of GMTex in the pressed state were therefore used in the FE material model.

The most important properties of the PP GMTex materials are summarized in Table 4 along with the values for common LFTs and GMT without woven layers. It can clearly be seen that the GMTex had superior properties compared to other materials.

Table 4. GMTs and LFTs used to develop hybrid forming.

GFRP	Max. Tensile Stress [MPa]	Tensile Modulus [MPa]	Max. Tensile Strain [%]
PP GMT 40% GF	85	6100	1.95
PP GMTex 40% GF	235	11,200	2.6
PP GMTex 60% GF	380	18,600	2.3
PA6 LFT 40% GF	160	10,600	2.5
PP LFT 40% GF	100	9100	2

For bonding strength tested using shear and cross-tension testing according to Section 2.2 (Figure 3), an average shear tensile strength of approximately 6 MPa and a cross-tension strength of around 3.5 MPa were measured. The failure mode exhibited adhesive failure, with the adhesive primer remaining on the aluminum sheet. These strength values and the corresponding force–displacement curve (see Figure 11) were used to calibrate the model parameters of MAT 240 as described above in Section 2.6.

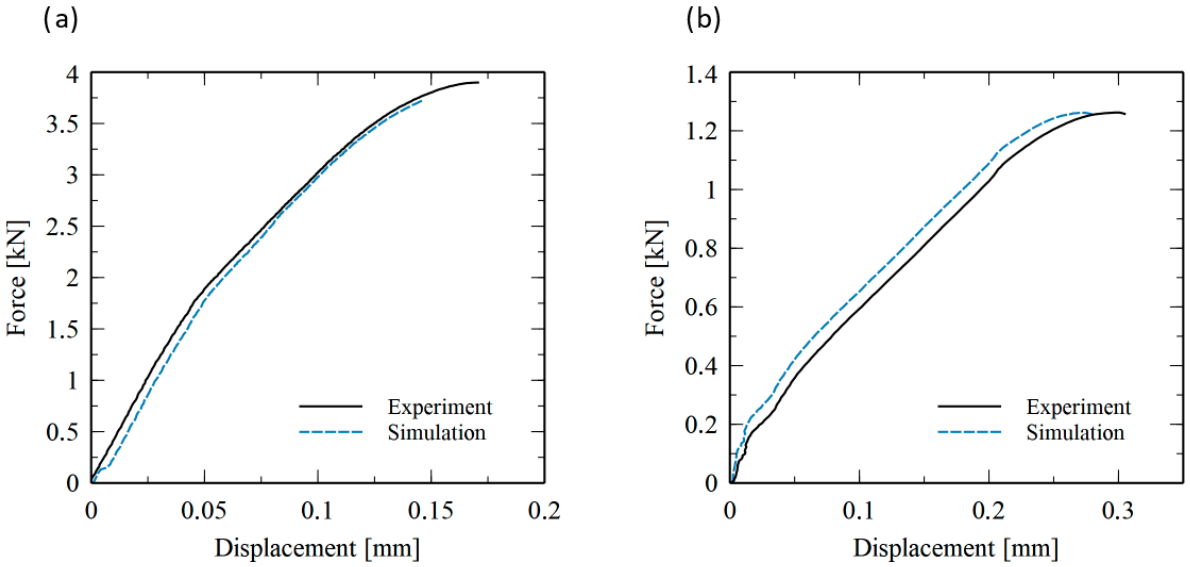


Figure 11. Fitted force–displacement curves from the reverse-engineering FEM model: (**a**) lap shear and (**b**) cross-tension.

4. Design of the Hybrid Crash Box of the CMS

After the properties of the reference CMS and the properties of the materials to be used in the hybrid CMS were determined, the hybrid CMS was subsequently designed and optimized.

4.1. Crash Box Design and Optimization

To find the optimized crash box design using the Al–GMTex system, four rib geometries with pure GMTex material (see Figure 12a) for a single-hut U-profile were examined first: honeycomb, X cross, pattern, and orthogonal. A rib height of 25 mm and a constant GMTex layer thickness were selected for all variants. The rib thickness for all variants was 3.8 mm in the longitudinal and 3.5 mm in the transversal direction. From the FEM model calculated using the method described in Section 3, the force–displacement curves of these rib structures and their energy absorption were calculated and are shown in Figure 12b.

It can be seen that of all rib variants considered, the orthogonal GMTex rib structure produced the best performance in axial crash simulation in terms of energy absorption for a given input energy. Therefore, the orthogonal rib structure for the crash box design was considered for further geometrical parameter studies. The parameters that were considered for optimization are indicated in Figure 13, where the investigated double-hut profile is shown (the geometry of the profile is different from that in Figure 12a). Table 5 shows the parameter ranges at which the parameters were systematically varied. The goal was to attain a homogeneous force–displacement curve.

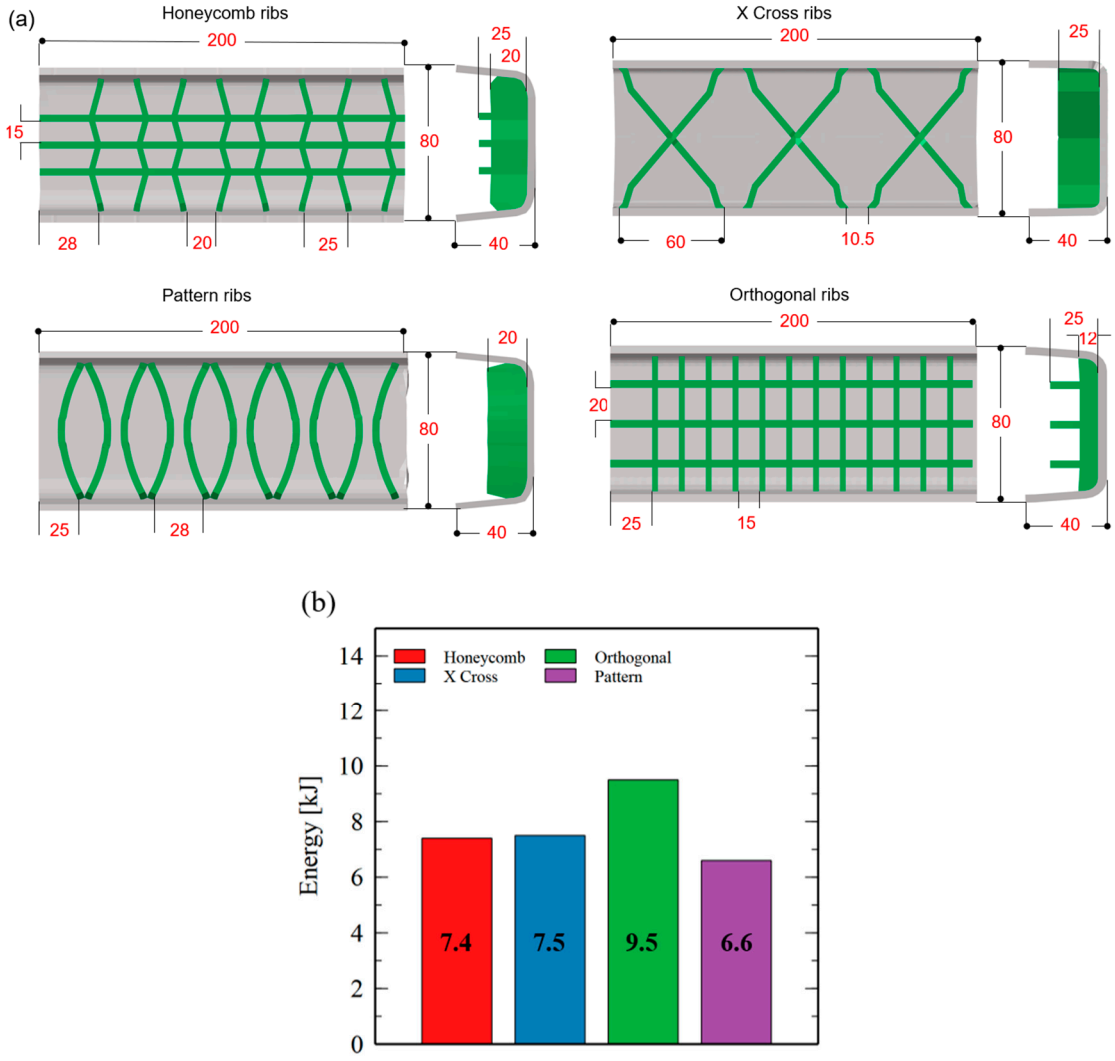


Figure 12. (**a**) Investigated rib geometries; (**b**) comparison of energy absorption of different rib structures (single-hut).

Table 5. Parameter ranges of orthogonal rib structures.

Parameter	Range of Values for Parameter [mm]
Transversal rib height (TH)	5–12–15
Transversal rib thickness (TT)	2.5–3.5–4
Transversal rib distance (TD)	15–20–25–30
Longitudinal rib height (LH)	30
Longitudinal rib thickness (LT)	3.5–4–4.5
Longitudinal rib distance (LD)	20

The geometric limits were defined based on the observed material flow and fiber-filling behavior of GMTex in thin rib structures, and on parameter boundaries reported in previous studies in ref. [45]. These constraints ensure that all optimized geometries remain manufacturable and structurally meaningful.

The FEM model was built as described in Section 2.6. An input energy of 9.8 kJ was defined in the simulation by applying a load of 1000 kg to the impactor and giving an initial velocity of 4.44 m/s to the impactor in the positive Y direction. This corresponds to the test speed for the RCAR 10° low-speed structural crash test. The force–displacement curve and the specific energy absorbed were studied for each iteration, and the geometrical change

for the following iteration in the design was decided. The goal was to achieve an extreme constant (high) force level with maximum specific energy absorption (*SEA*).

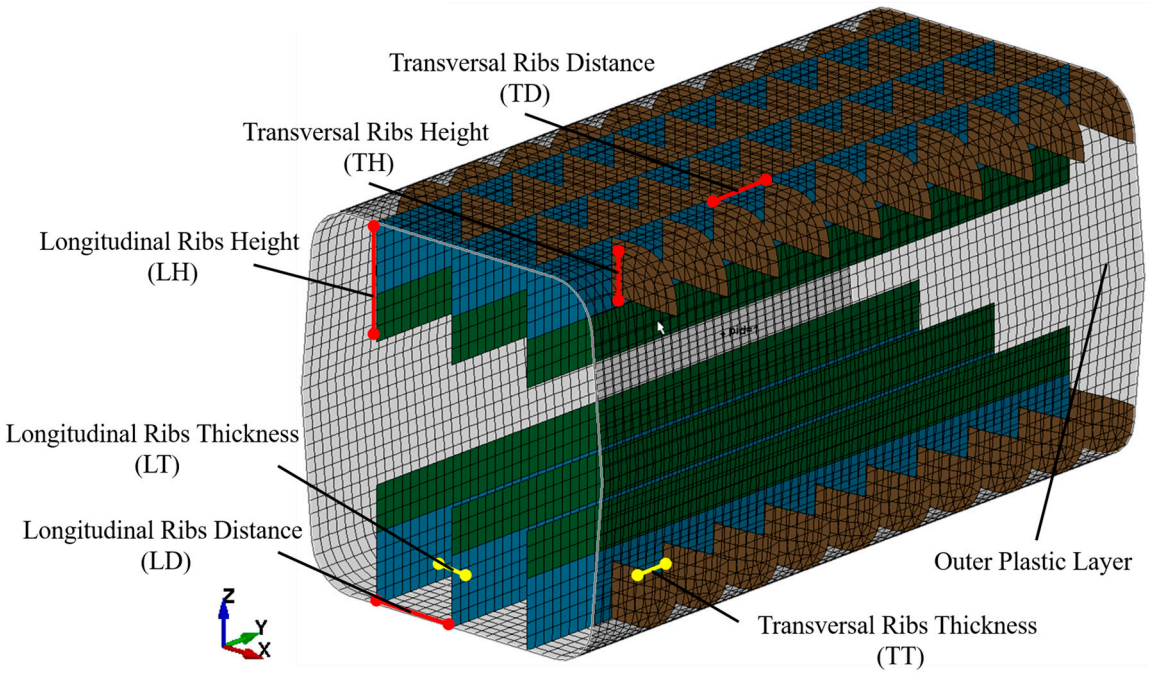


Figure 13. Geometric parameters of the crash box for design optimization.

The force–displacement curves of a few iterations listed in Table 6 are shown in Figure 14a, with the nomenclature given in Table 6. On comparing the performance of crash box versions CB5 (gray curve) and CB3 (green curve), both crash boxes have the same initial peak generated when the falling mass contacts the crash box and also a similar mean force level. However, the second peak of the CB5 at approx. 20 mm displacement is considerably higher than the first peak, which is not desirable. This could be because the increased transversal rib height of 15 mm produces a stiffer crushing effect than that of CB3. On comparing the crash box versions CB3 and CB1 (red curve), it can be seen that the initial peak of the CB1 version is lower than that of CB3, which can be attributed to the reduction in longitudinal rib thickness in CB1. The reduced transversal rib height of 5 mm and transversal rib thickness of 2.5 mm are not stiff enough to produce a higher mean force level.

Table 6. Selected parameters of five crash box geometries.

	TH [mm]	TT [mm]	TD [mm]	LH [mm]	LT [mm]	LD [mm]	Mean Force Level [kN]
CB1	5	2.5	15	30	3.5	20	52.8
CB2	5	3.5	15	30	3.5	20	58.8
CB3	12	3.5	15	30	4.5	20	72.2
CB4	12	2.5	15	30	4.5	20	69
CB5	15	3.5	15	30	4	20	76

Figure 14b shows the *SEA*, which is the ratio of the energy absorbed per weight of the crash box. Variants CB1, CB2, and CB4 showed similar *SEA* of approx. 24 kJ/kg. However, here, synchronous with the performance in terms of force–displacement curves, it can be seen that CB3 produced the best *SEA* (about 27 kJ/kg) compared to all the other crash boxes. CB5 had an *SEA* quite close to that of CB3. However, CB5 shows a very strong

second force peak and thus lower homogeneity of forces. Therefore, CB3 was considered the best variant.

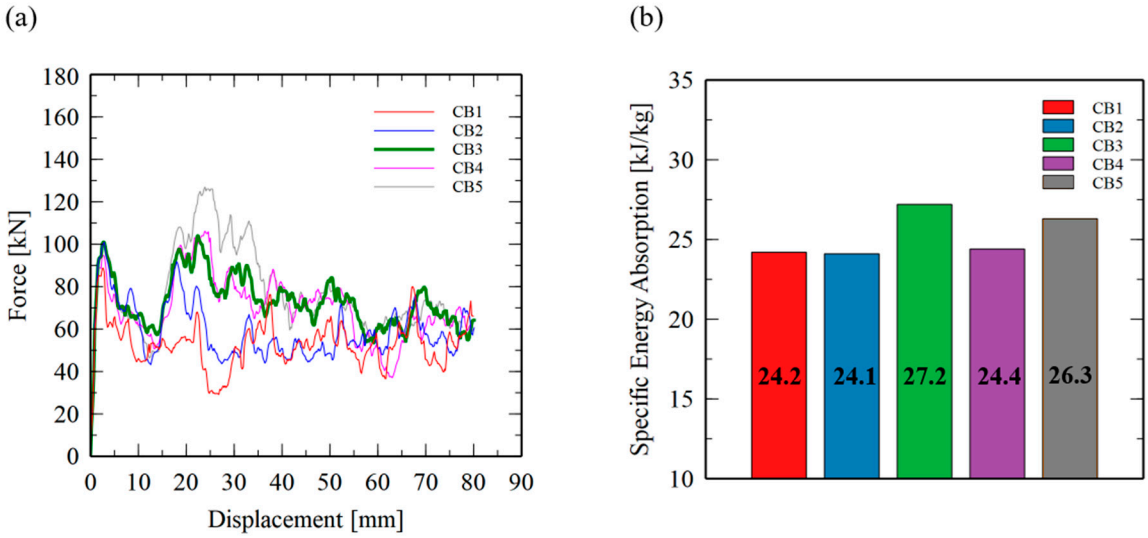


Figure 14. (**a**) Force–displacement curves and (**b**) *SEA* of five pure double-hut GMTex crash box variants.

Figure 15 shows the crushing morphology in the simulation of the selected crash box variant 3 at different crushing displacements. At a crushing displacement between 0 and 5 mm, the impactor contacts the outer layer and the longitudinal ribs, where the longitudinal ribs bend, as can be seen in (1) in Figure 15b, and generate the initial peak (1) in the force–displacement response in Figure 15a. After this initial contact, the longitudinal ribs fail, leading to a reduction in the load until the impactor subsequently engages with the transversal ribs. Between 15 and 20 mm displacement, the second peak occurs, where the impactor contacts the first transversal rib (see (2) in Figure 15a,b). The debris seen are the elements that were deleted due to the material failure in the FEM model. Consequently, on further continuation of the simulation, peaks are achieved when the impactor contacts both longitudinal and transversal ribs simultaneously. The major load drops observed in the force–displacement curve correspond to the sequential failure of the transversal ribs during axial crushing, as shown in peaks (3) to (5) and their corresponding failures.

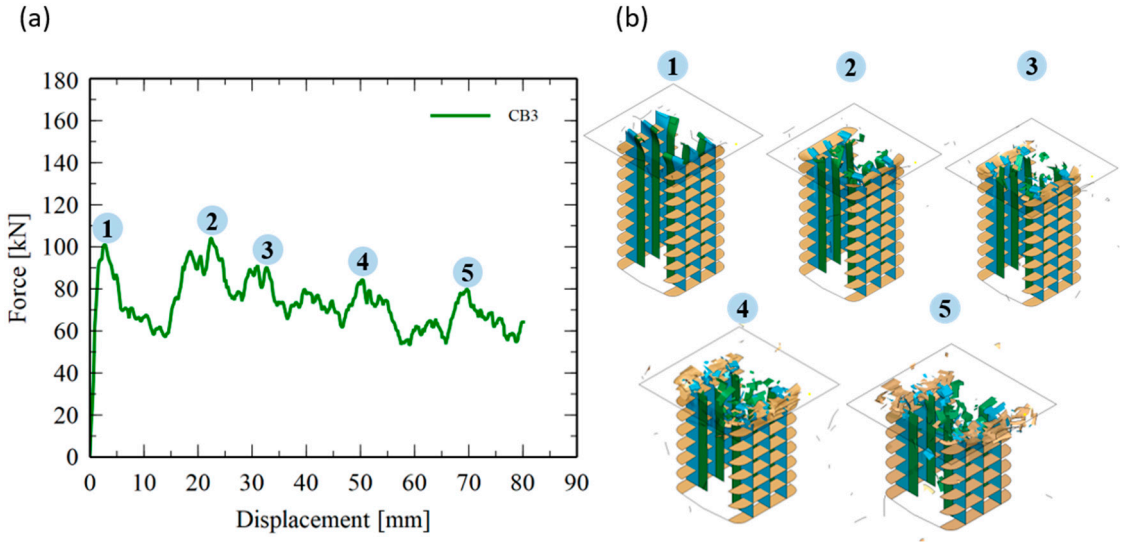


Figure 15. (**a**) Crushing morphology of the selected pure double-hut GMT crash box variant 3, and (**b**) the corresponding failure mechanisms in stages 1 to 5.

The selected CB3 rib geometry was used to produce both pure GMTex and Al–GMTex hybrid crash boxes, assuming that Al sheet metal will not influence the GMTex behavior. In the manufacturing of hybrid crash boxes using the hybrid forming process, the GMTex is located in the inner area of the crash box. This ensures that a crash box absorbs energy very efficiently through deformation of the Al and crushing of the GMTex. Since the GMTex is covered by the Al sheet metal shells, no portions of the GMTex material could be shattered outside of the crash box during a crash event.

4.2. Crash Box Manufacturing and Evaluation

Using the tool and sealing concept described in Section 2.3, the pure GMTex and Al–GMTex hybrid crash box developed in Section 4.1 were manufactured and analyzed. Figure 16a shows the hybrid-formed Al–GMT crash box. Since the tool was designed for a total hybrid crash box thickness of 3.5 mm, the thickness of the pure GMT crash box was also 3.5 mm, consisting of a 1.5 mm Al sheet and a 2 mm GMTex layer.

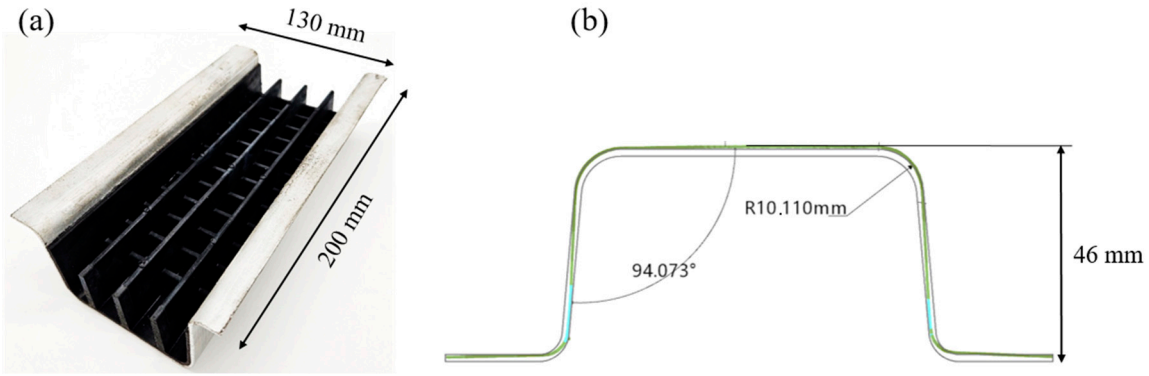


Figure 16. (**a**) Hybrid-formed crash box with aluminum and GMTex, (**b**) 3D scan to compare the geometric deviation between the CAD (black) and the formed part (green).

Subsequently, the forming of the AA5182 alloy was analyzed using a 3D scan arm from Faro. The deviation between the formed Al sheet surface and the CAD model of the die was determined, as shown in Figure 15b. The results show that the Al alloy was almost perfectly formed in the radius area (R = 10.11 mm) with a small deviation of 0.11 mm from the CAD geometry (R = 10 mm).

In addition to the forming of the Al alloy, the warpage of the hybrid profile due to thermal residual stresses was investigated. Generally, warpage in hybrid components results from volumetric shrinkage of the plastic components and cooling of the metal component after hybrid forming. The thermal expansion coefficient difference is a key factor. In the case of the Al–GMTex hybrid in this study, their thermal expansion values were within a comparable range, which suggests advantages in terms of geometric warpage compared to steel. The warpage of the Al–GMTex crash box geometry is shown in Figure 16b. The hybrid crash box shows an opening angle of 94.073° and thus deviates approx. only 1% from the 95° die opening angle. The opening angle of manufactured hybrid crash boxes is smaller than the die angle due to GMT shrinkage. As a result, the aluminum sheet is pulled inward.

The forming of the GMTex layer can also be evaluated using the thickness distribution of the component at various cross-sections. The results of this analysis are shown in Figure 17. It shows a consistent GMTex thickness distribution of 2 mm in almost all cross-sections, with small deviations in localized areas. These small variations were presumably caused by the placement of the GMT into the tool. Additionally, a thinning of the aluminum sheet from 1.5 to 1.4 mm due to sheet metal forming can be observed.

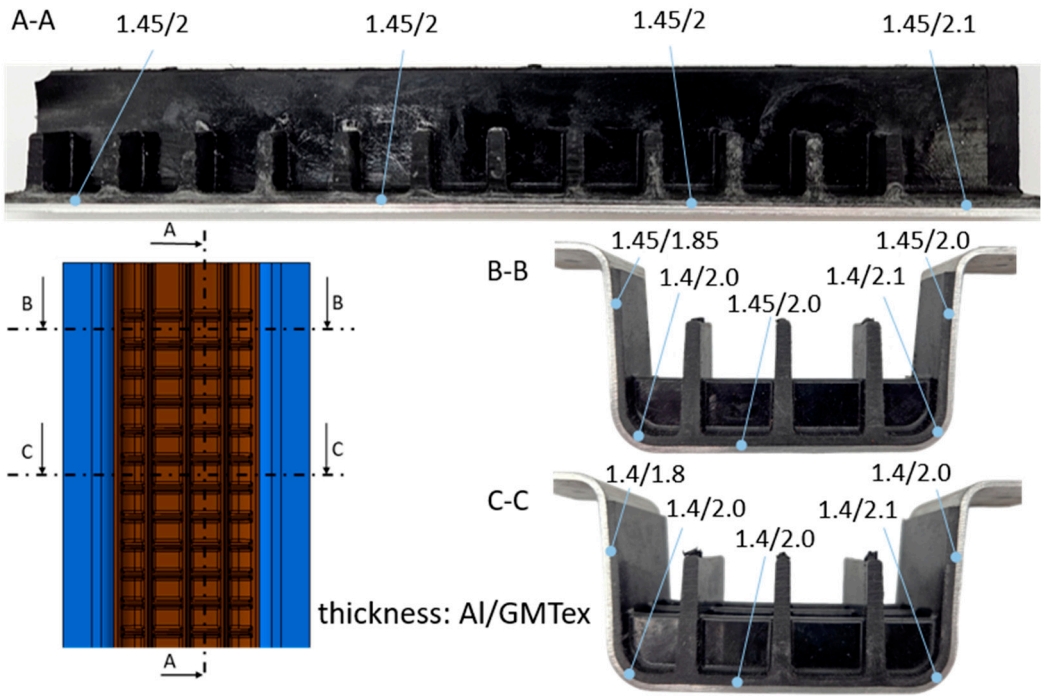


Figure 17. Manually measured AA5182-GMT thickness.

4.3. Dynamic Drop Tower Test

To determine the deformation and failure behavior of GMTex and Al–GMTex hybrid structures under high-speed loads, both GMTex and Al–GMTex hybrid crash boxes were manufactured and tested in drop tower tests using only the single-hut profile as described in Sections 2.4 and 4.2.

To initiate progressive failure in GMTex and reduce the initial peak force, a local structural trigger in the form of a 45° chamfer was introduced at the top of the component in the developed geometry [46,47]. This trigger weakens the structure locally and allows the crash box to form a constant crash front, preventing failure due to instability. The representative results of the drop tower tests for pure GMTex crash boxes with and without a 45° chamfer are shown in Figure 18.

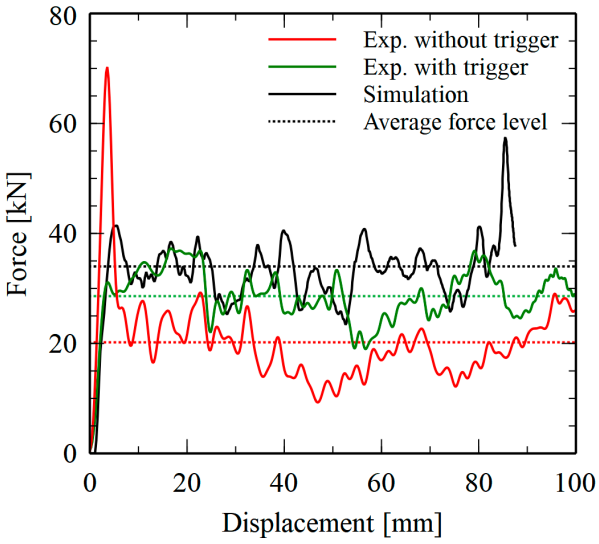


Figure 18. Comparison of simulated and experimental force–intrusion curves of a pure single-hut GMTex crash box with and without a 45° chamfer trigger.

Analyzing the crushing behavior of the GMTex crash box (single-hut U-profile) shown in Figure 18, several characteristics of the force–displacement (*F-s*) curve can be derived. The *F-s* curve with chamfer shows that the GMTex crash box exhibits little force variation after the initial peak force, resulting in excellent energy absorption up to approx. 100 mm. This continuous energy absorption is a result of fiber and matrix fractures as well as delamination of layers [48]. As expected, the initial peak force for the crash box without a 45° chamfer is much higher. This leads to unstable damage in the longitudinal side wall area of the crash box after approx. 10 mm of intrusion (Figure 19a). As shown in Figure 19a, larger fragments can be seen near the impact area, so that not the entire cross-section but only partial areas contribute actively to energy absorption. The corresponding deformation and fracture pictures of the crash box with the chamfer are shown in Figure 19b. At 10 mm up 40 mm displacement, it shows more homogeneous behavior.

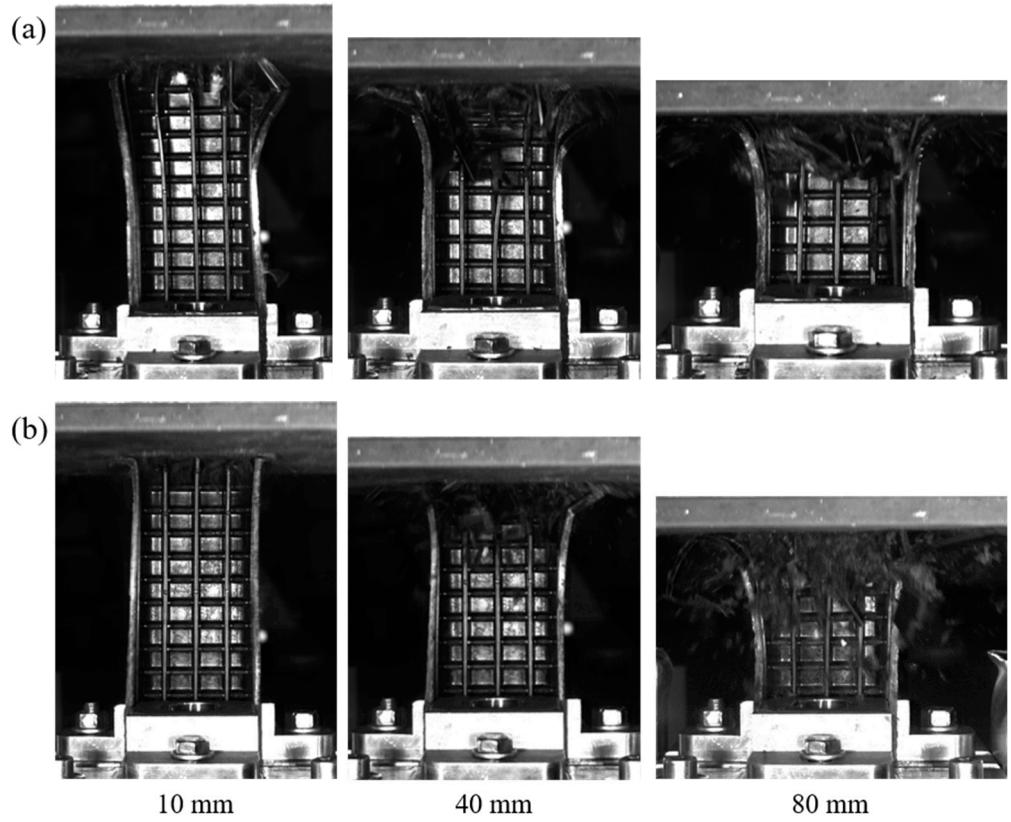


Figure 19. Sequential illustration of component failure during drop tower test (**a**) without and (**b**) with trigger.

The average *F-s* curves were also calculated and are depicted in Figure 18. A comparison of the average force levels shows a difference of approx. 28% between both variants. Based on the experimental data obtained, the *SEA* of the samples with the trigger is calculated as follows:

$$SEA = \frac{E_{abs}}{m_{crush}} \quad (1)$$

and

$$E_{abs} = \int_0^s F(s)ds \quad (2)$$

with the absorbed energy E_{abs}, the resulting force F as a function of impactor intrusions, and the destroyed component mass m_{crush}. The crushed mass is estimated by the cross-sectional area of the crash box and the maximum intrusion of the impactor. With a total absorbed energy of 3 kJ and a determined destroyed mass of 0.092 kg, the *SEA* of the GMTex crash

box is calculated to be 31.4 kJ/kg. This value is 25.6 kJ/kg for the crash box without the chamfer. Both values exceed the *SEA* of the steel thin-walled tube of 18.5 kJ/kg reported in the literature [49].

To provide a quantitative assessment of the model accuracy, Table 7 summarizes the key performance metrics of the experiment with trigger and the simulated force–displacement response. The simulated mean force shows a deviation of 13.7% while the maximum crushing displacement differs by 18%. The total energy absorption is nearly the same. Despite these deviations, the overall shape of the force–displacement curve and the progressive crushing behavior are captured with good fidelity, confirming the suitability of the MAT54 model for predicting GMTex crushing behavior.

Table 7. Comparison of the experimental and simulated crash response of the pure GMTex crash box.

Parameter	Experiment with Trigger	Simulation
Initial peak force [kN]	29 ± 4	41
Mean force level [kN]	28.5 ± 0.7	33
Max. intrusion [mm]	104 ± 5	88
SEA [kJ/kg]	31.4 ± 0.2	32.3

After testing the pure GMT crash boxes, drop tower tests with hybrid Al–GMTex crash boxes were carried out. Figure 20a shows the deformation and failure behavior of hybrid crash boxes. The energy absorption of Al is carried by the fold pairs in the crash zone due to its ductility. The deformation of GMT behind Al sheets cannot be followed during the crash event. The energy absorption of the hybrid components is assumed to be a combination of Al folding and the crushing of GMTex and is further analyzed by the FEM.

The crash behavior can also be observed in the *F-s* diagram in Figure 20b. Due to the use of a "double" U-formed crash box and the additional Al shells in the Al–GMTex hybrid, the *F-s* curves are more than double those in Figure 18. In both the experiment and the simulation, there are five fold pairs, as marked on the crashed component in Figure 20a. It can be seen from the experiment that the process stops before the fifth fold pair is completed, as the total impact energy has already been absorbed. The *F-s* curve in simulation slightly exceeds the experimental values at deformation up to 60 mm, and the overall simulation result is satisfactory (see Figure 20b).

Further comparison shows that the force level increases significantly from 60 mm displacement in the experiment, while it drops sharply in the simulation. This discrepancy results from the fact that in the experiment, GMT is completely enclosed by the aluminum, and the broken GMT fragments remain in the hybrid crash box during the crash test. In contrast, in the simulation, all fragments are deleted after reaching the failure criterion and cannot further contribute to energy absorption. Therefore, the simulated force level was lower compared to the measured values for larger deformations.

With a total absorbed energy of 7 kJ and an estimated destroyed mass of 0.21 kg, the *SEA* of the hybrid crash box is calculated to be 32.5 kJ/kg. In summary, hybrid crash boxes provide the same *SEA* as pure GMT crash boxes. Concerning energy absorption, a hybrid crash box does not show an advantage. However, it prevents GMT fragments from affecting the environment during a crash event. A comparative summary of *SEA* values for aluminum, pure GMTex, and hybrid crash boxes is provided in Figure 21 to highlight the relative energy absorption capabilities.

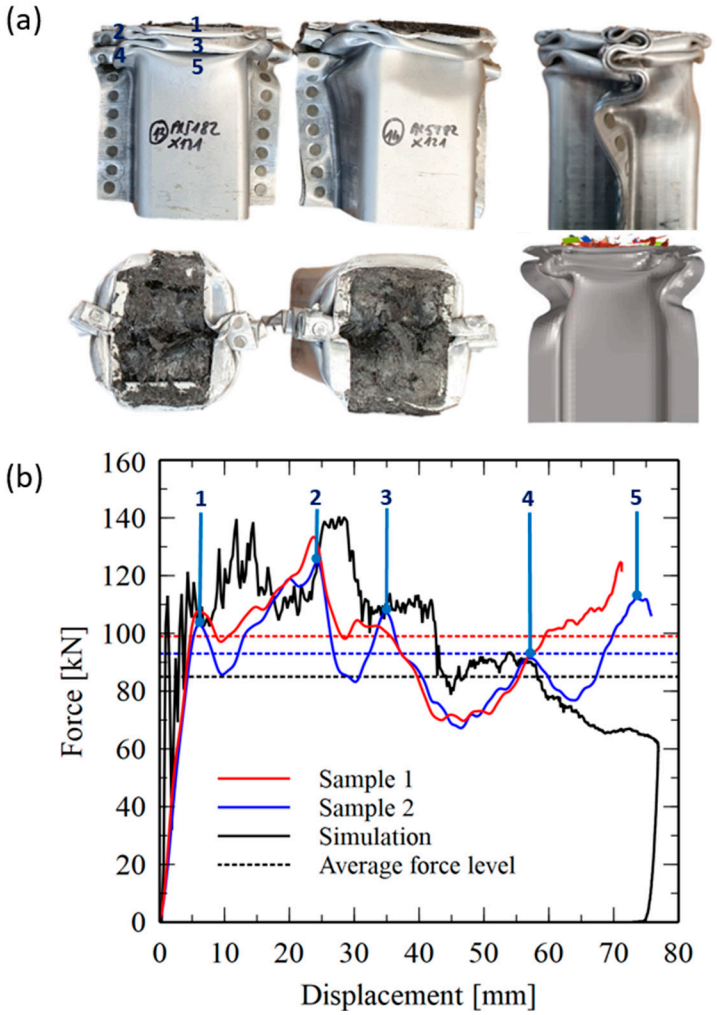


Figure 20. (**a**) Deformed Al–GMT hybrid crash box and FEM-predicted results after impact; (**b**) comparison of experimental and simulated force–intrusion curves.

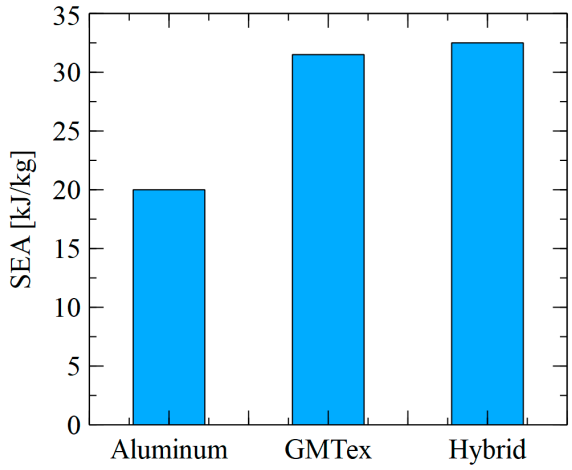


Figure 21. Comparison of *SEA* of aluminum, pure GMTex, and hybrid aluminum–GMTex crash boxes.

A quantitative comparison of the Al–GMTex hybrid crash box is summarized in Table 8. The simulated mean force differs from the experimental Sample 2 value by 8.6%, while the peak force shows a deviation of 4.6%. The maximum crushing displacement agrees very well, with only 1.3% difference between simulation and experiment. The close agreement in mean force level, peak behavior, and maximal displacement confirms that the combined

MAT 24–MAT 54–MAT 240 modeling approach reliably predicts the crushing response of the hybrid crash box.

Table 8. Comparison of the experimental and simulated crash response of the hybrid crash box.

Parameter	Experiment	Simulation
Initial peak force [kN]	104 ± 4	113
Mean force level [kN]	96 ± 5	85
Max. intrusion [mm]	73.5 ± 3.1	77
SEA [kJ/kg]	32.5 ± 2.3	32

For a detailed analysis of the energy absorption mechanisms in the hybrid crash box, cross-sections of the components were examined. The aim was to investigate the extent to which the energy absorption mechanisms of hybrid components correspond to those of the individual components. Figure 22a shows a cross-section of the hybrid crash box parallel to the longitudinal axis of the component. Both the aluminum and the GMTex parts behave as they would in pure structures. As mentioned above, failed GMTex parts are fixed by the enclosed aluminum and do not shatter outside the aluminum profile (compared to Figure 19). The main energy absorption mechanisms of the GMTex part are identified as local buckling, rupture, and delamination, parallel to the folding for the Al part of the crash box, with the delamination occurring mostly as bending towards the inside of the component. As shown in Figure 22a, although the GMT structure is still bonded to the Al sheets below the crushing zone, separation of bonding between the Al and GMT can be observed in the crushed region.

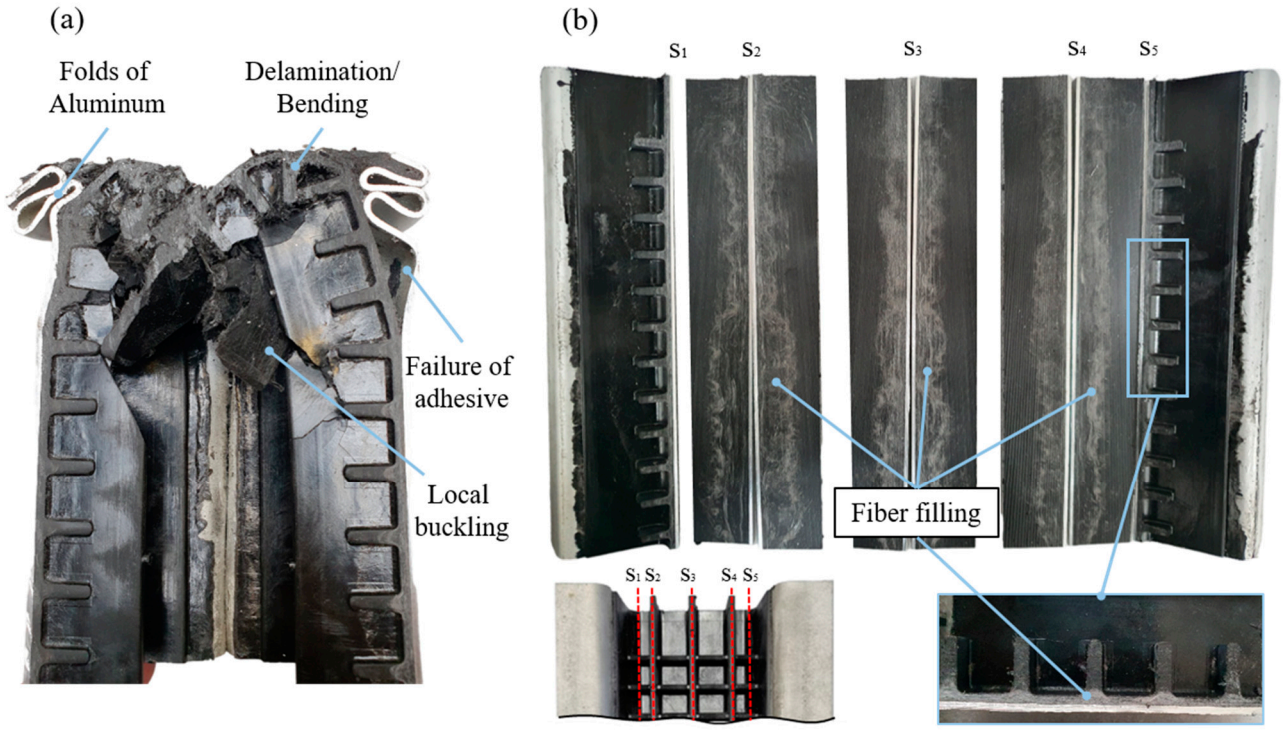


Figure 22. (**a**) Cross-section of the hybrid crash box after impact; (**b**) several cross-sections of the crash box specimen in the longitudinal and transversal directions, showing fiber filling.

Furthermore, the fiber filling could be examined in the cross-section views (Figure 22b). An inhomogeneous fiber distribution can be seen in both the longitudinal and the transversal ribs. It can be seen that the lower part of the ribs is filled with fibers and matrix, while the upper part contains only the pure matrix. This could be due to the stacked plies and woven

fabrics of GMTex material in the lower area of the component during manufacturing, which obstruct fiber filling. In ref. [38], the details of fiber filling of GMTex materials in different zones of a similar u-profile to this work were reported based on microscopic imaging and CT analysis. These results were used as input into the simulation and considered during the modeling of hybrid components in this work.

4.4. Intermediate Conclusions on Crash Box Development

The analyses conducted in Section 4 lead to several important conclusions regarding the crash performance of both pure GMTex and aluminum–GMTex hybrid crash boxes:

1. Rib structure optimization: The orthogonal rib configuration (CB3) demonstrated the most favorable balance of high specific energy absorption (*SEA*) and homogeneous force–displacement behavior, making it the optimal pure GMTex reference design.
2. Behavior of pure GMTex crash boxes: Pure GMTex crash boxes exhibited highly progressive crushing behavior with low force fluctuations when an appropriate trigger was applied. Their *SEA* values exceeded those of conventional metallic crash boxes; however, fragmentation and material ejection were observed, which limits their direct applicability in automotive crash structures.
3. Behavior of hybrid aluminum–GMTex crash box: The hybrid crash boxes achieved *SEA* values slightly higher than pure GMTex, as shown in Figure 21, and offered significantly greater deformation stability. The aluminum shell confined the GMTex fragments, ensured controlled folding, and prevented debris from escaping the profile. This improves functional robustness and makes the hybrid design more practical for real vehicle integration.
4. Simulation-Experiment agreement: The finite element simulations reproduced the folding sequence, load levels, and energy absorption characteristics with good consistency, confirming the suitability of the calibrated material and cohesive-zone models.

Overall, the results show that while pure GMTex exhibits excellent intrinsic energy absorption, the hybrid design provides superior structural stability and integration capability, making it a more viable solution for inclusion in the hybrid CMS described in Section 5.

5. Design and Optimization of Al–GMT Hybrid CMS

After the design of the crash box as part of CMS was established in Section 4 for pure axial loading, the entire hybrid CMS was subsequently developed using FEM.

5.1. Design of the Crash Box as Part of CMS

Since the orthogonal rib pattern in Section 4 was only investigated under axial loading, further optimization steps regarding the RCAR 10° low-speed structural crash test for the entire CMS design were necessary. The crash box in the entire CMS also had to ensure maximum energy absorption when the CMS is crashed at a 10° angle. Figure 23 shows the detailed development steps. Through simulation, the Al sheet thickness for both the crash box and the cross-member was predefined at 1.5 mm to prevent damage to the Al sheet during GMT crushing.

At first, the GMTex layer was determined. The optimization of the large-area GMTex layer and the GMT rib structure was carried out through manual optimization using the FE models described in Section 2.6. According to industry manufacturing guidelines, the GMT layer thickness should not be less than 2 mm. Therefore, it was initially defined as 2 mm. The available cavity inside the component was used to design the rib structure. In the first optimization step for the RCAR 10° test, the crash box was additionally reinforced in the region where the first contact between the crash box and a rigid wall occurs. In contrast to the geometry developed in Section 4.1, the GMTex reinforcement consists of different

thicknesses in different areas. Figure 24a shows the resulting GMT reinforcement of the crash box with varying thicknesses due to the asymmetry of the load bearing of the crash box at 10° loading. It increases from 2 to 3 mm to enhance the energy absorption of the CMS. The thickness of the longitudinal ribs is 4.5 mm, and the transversal ribs are 3.3 mm at the rib base. The upper corner of the GMTex has a chamfer to reduce the initial force peak and to initiate a progressive failure of the GMTex.

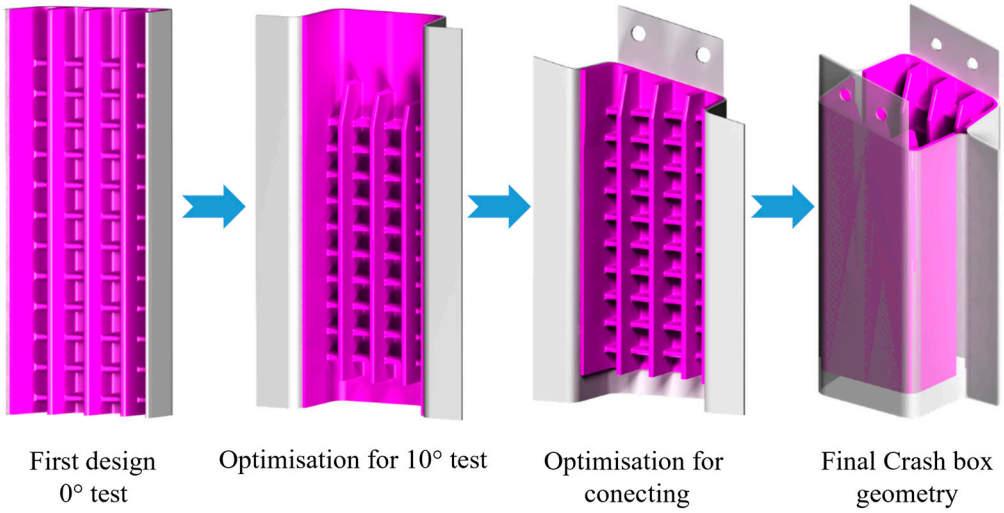


Figure 23. Development of the Al–GMT crash box geometry for the RCAR 10° structure test: optimization steps.

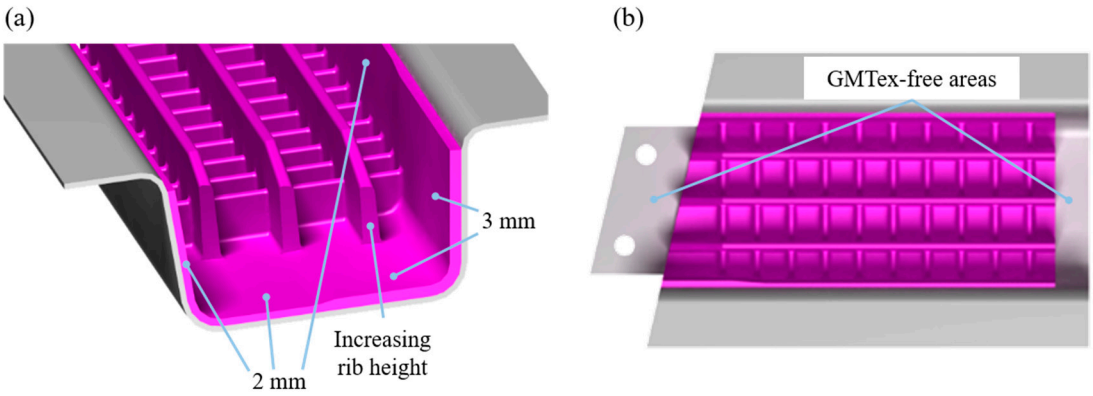


Figure 24. (**a**) Optimized crash box geometry and (**b**) final crash box with GMT-free areas.

Optimal connection between the crash box and cross-member is of crucial importance for the assembly of the CMS. A self-piercing riveting technique was employed to join the two halves of the hybrid crash boxes using the flange of the profile, as shown in Figure 20a, since welding of the hybrid parts is currently not feasible. Additional mass was added due to the flange. The crash boxes and cross-member had to be bolted together, as welding the two hybrid components is not yet reliable due to the adhesive and GMTex.

In order to be able to screw them, the crash boxes must be cut to their final contour (see Figure 24b) by an abrasive 3D waterjet technique on a five-axis waterjet machine. Waterjet processing was approved in refs. [50,51] as being well suited for mechanical processing of FRP, since it is a cold-cutting process.

5.2. Design of the Cross-Member as Part of CMS

While energy is almost exclusively absorbed by the energy absorber (crash box) during the RCAR 10° low-speed structural crash test, in the RCAR bumper compatibility test (see

Section 2.5), energy absorption is primarily achieved through the bending of the cross-member. The intrusion of the cross-member should be as low as possible to minimize repair costs [3].

During the RCAR bumper test, local buckling occurs in the middle of the cross-member, significantly increasing the intrusion. Thus, the hybrid cross-member must be optimized with the corresponding GMTex reinforcement while achieving the weight reduction target of 20%. Figure 25 shows several development steps of the cross-member for this test.

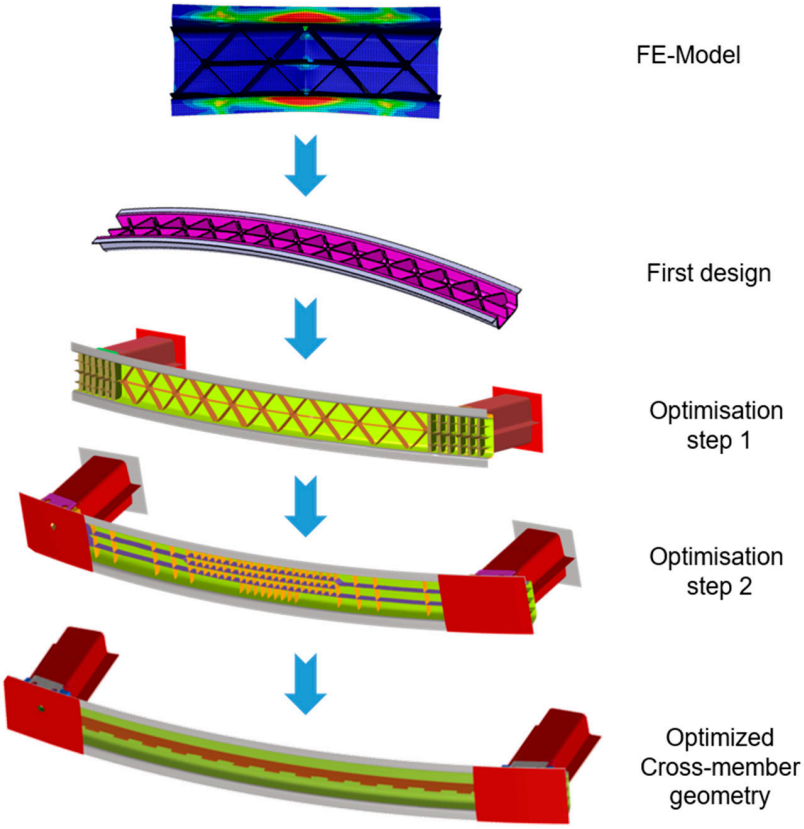


Figure 25. Development of the Al–GMT cross-member geometry: optimization steps.

First, cross ribs were introduced in the middle of the cross-member, as they provide high stiffness under bending and torsional loads. Since the fiber filling in the GMTex ribs is very restricted, as shown in Figure 22b, the rib height was designed to be only 15 mm. With this design, the intrusion and torsion of the cross-member were too large. Therefore, GMTex cross ribs in the middle area of the cross-member were optimized using topology optimization (Figure 25, step 2). However, the obtained geometry was too heavy. To reduce the weight of the cross-member, the GMTex ribs were replaced with one longitudinal rib made of UD fiber-reinforced tape according to Section 2.1 (Figure 25, optimized geometry). The final version of the pattern ribs with a middle UD tape achieved high stiffness in bending and torsion with the potential of up to 20% weight reduction compared to the reference Al-CMS. This was therefore selected as the final rib geometry for the cross-member. This achieved the optimal properties, as the UD tapes used have significantly higher compressive strength than GMTex.

In order to solve the issue of cross-member torsion during the RCAR bumper test, the developed concept also incorporated C-clamps (Figure 26). The thickness of the C-clamps was optimized through FE simulation to minimize weight. The C-clamp significantly reduced the cross-member torsion and thus the intrusion during the RCAR bumper test, as shown in Figure 27. Although the C-clamp reinforcement improves the structural stiffness

of the CMS, it introduces an additional mass of 280 g that must be considered in relation to the light weighting target.

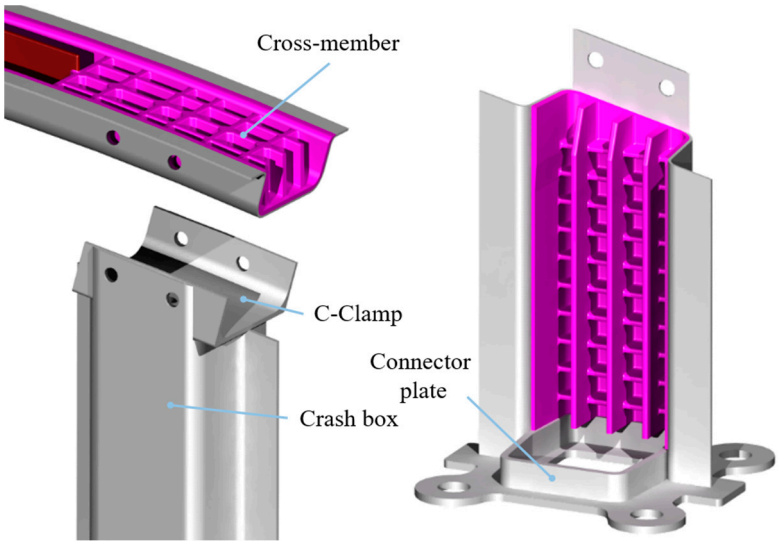


Figure 26. Connection of crash box cross-member and crash box by a C-clamp and connection to front rails using a connector plate.

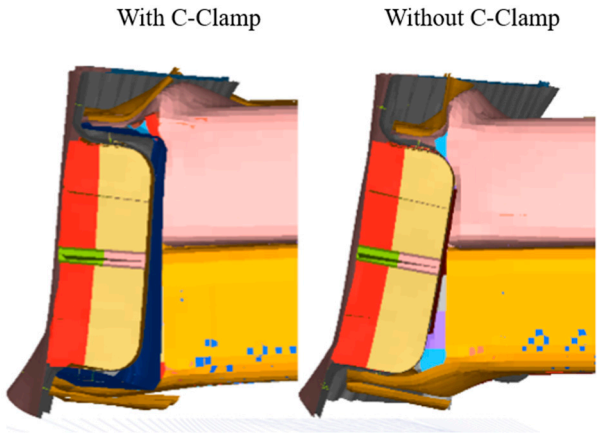


Figure 27. Reduction in torsion by adding a C-Clamp.

Additionally, due to the difficulty of welding Al–GMTex hybrid components and due to the reduced cross-member and crash box sheet thickness, the C-clamp provides a good alternative for the attachment of the tow hook. For tow hook design, the load cases shown in Table 9 were applied. Figure 28 shows the FE model for the towing load case, where the towing key was fixedly connected to the C-clamp. Subsequently, different loads were applied to the towing key at various load angles, as shown in Table 9.

Table 9. Different loading angles applied for towing load case: hybrid CMS.

Loading Angle [°]	Load [kN]
Pure tension	13
Tension 30°_to_left	13
Tension 30°_to_right	13
Tension 20°_towards_top	13
Tension 20°_towards_bottom	13

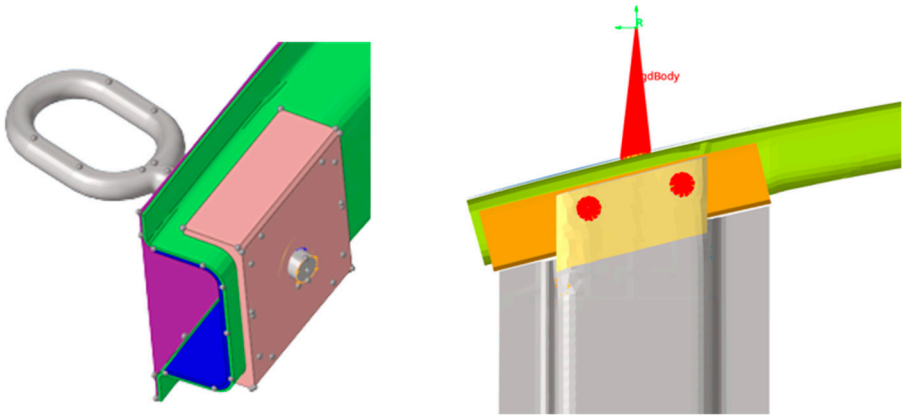


Figure 28. Towing load case in the hybrid CMS.

The hybrid CMS was optimized for the towing load cases at different angles so that the maximum permanent deformation was less than 3 mm. The von Mises stresses of the crash box in the connection area to the cross-member are compared in Figure 29. Under pure tensile loading, the stress is lowest. Tension at 20° towards the top and bottom shows the maximum stresses in the crash box due to eccentric loading. These were identified as the critical towing load cases. The C-clamp was optimized until the von Mises stresses in the crash box were below the yield strength of the Al alloy AA5182 used.

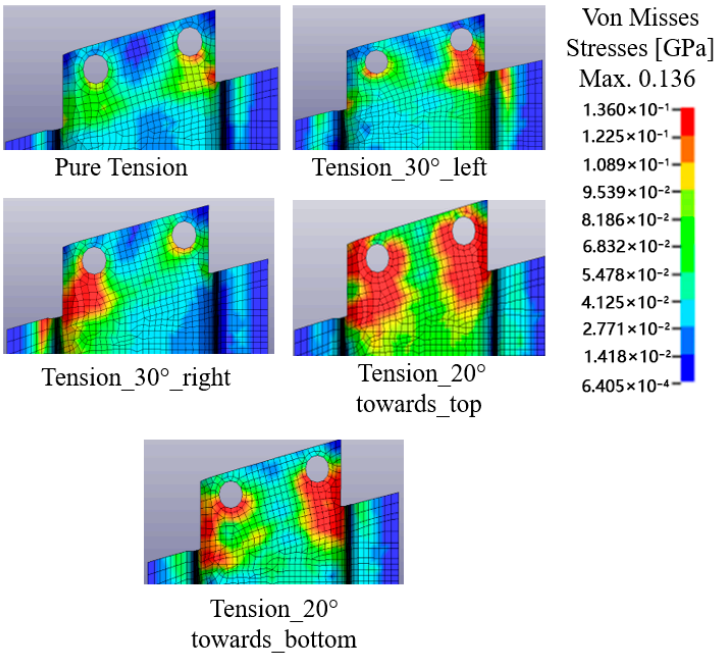


Figure 29. Stress distribution of crash box in different towing load cases.

Another challenge of the hybrid CMS is the connection between the crash box and the front rail of the car body. For this purpose, an additional connector plate was introduced (as shown in Figure 26) that can be screwed to another connecting plate welded in the front rail, as in the case of the reference CMS. In the reference CMS, the crash boxes are welded to the flange plate. Since welding generates high temperatures, at least for a short time, a minimum distance between the weld seam and the GMTex must be maintained. Therefore, GMTex-free areas were provided in the crash boxes (see Figure 24b). Subsequently, the hybrid CMS could be welded to the connector plate so that the entire hybrid CMS can be bolted to the front rail of the car body. Due to the weakness concerning welding, the weight of the crash box and

connection plate had to be increased. The entire assembly of the developed CMS is shown in Figure 30, including an Al closing plate with a very thin gauge of 4 mm.

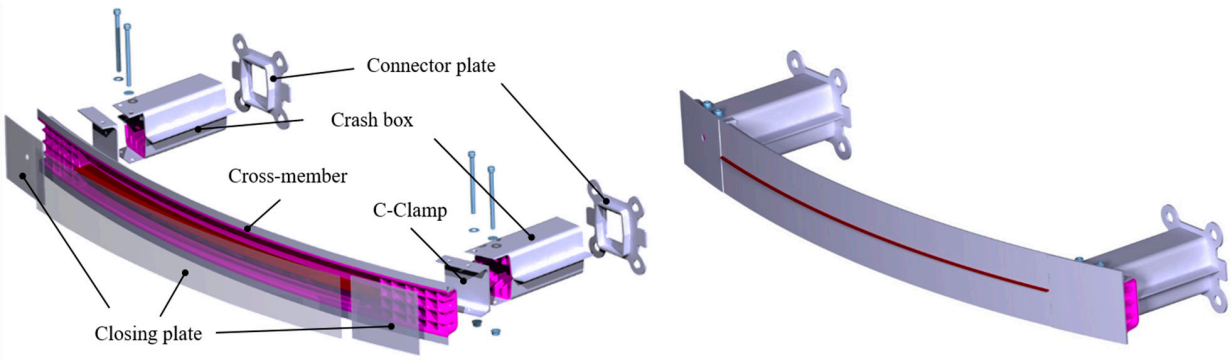


Figure 30. CAD assembly of the Al–GMT hybrid CMS.

Finally, the hybrid CMS was simulated using the material models described in Section 2.6. Figure 31a shows the simulation results of the force–displacement curves of the hybrid Al–GMTex CMS and the Ford Focus reference Al-CMS. Figure 31b illustrates the deformation behavior of the hybrid Al–GMTex CMS for the RCAR 10° low-speed structure test. It is noticeable that the first peak is significantly higher compared to the reference CMS, which is attributed to the stiff C-clamp reinforcement, and the force scatter of the first peak to the mean force level is larger than that of the Al-CMS. The reason is that the hybrid CMS combines two deformation mechanisms with different stiffness characteristics and failure modes. The aluminum forms discrete fold pairs, while the GMT layer undergoes progressive matrix failure and rib crushing, resulting in localized load drops followed by restabilization. These effects lead to a more oscillatory response. However, the resulting force level after the first peak remains relatively constant from approximately 35 mm to 85 mm intrusion. At 55 mm intrusion, the crash box deforms in the area where it is connected to the connector plate, leading to a temporary reduction in force level. Due to the geometry of the hybrid CMS, the average force level is approx. 10% higher than that of the reference. This leads to a reduction in intrusion in the simulation of about 8%.

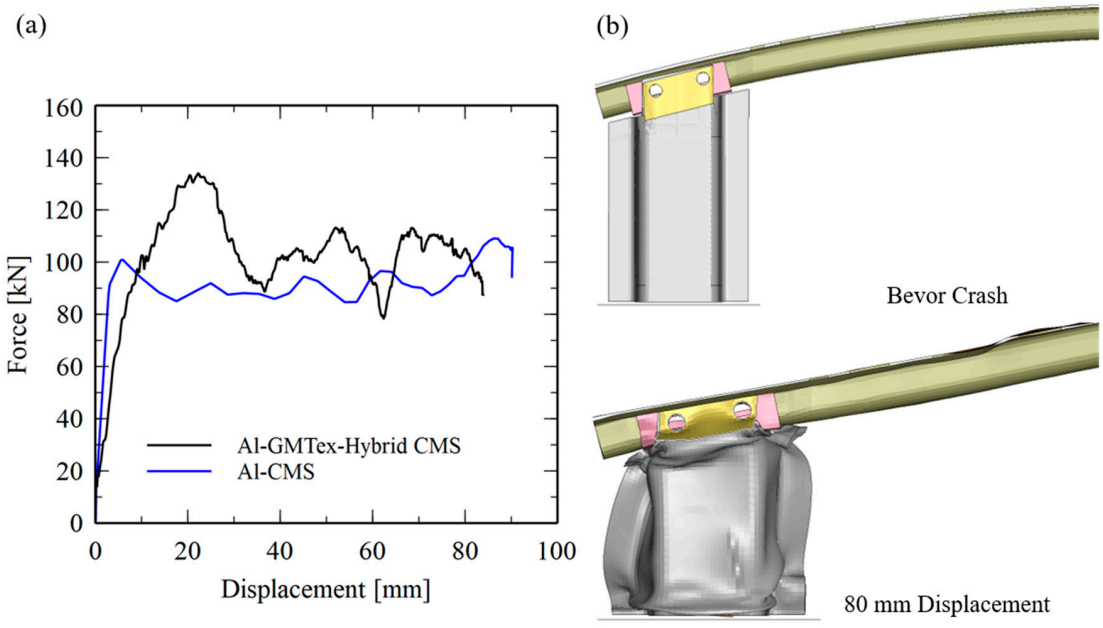


Figure 31. Simulation results: (**a**) RCAR low-speed structural test of reference Al-CMS and Al–GMT hybrid CMS and (**b**) FEM predicted results before crash and after 80 mm displacement.

Due to the flanges of the crash box for riveting the two half parts of the crash box and the added C-clamps, as well as the restrictions of welding the crash box and connector plate and the large screws used, the weight reduction of the crash box and cross-member was equalized so that the weight of the hybrid CMS was almost the same as that of the reference pure Al-CMS. The weight-saving potential of an Al–GMT hybrid CMS could not be utilized due to the joining technology.

6. Conclusions

Based on a previously developed hybrid forming process that enables the simultaneous forming of sheet metal and FRPs as well as the joining of these two materials, this study applied this technology to crash-relevant subassemblies. Numerical studies were carried out to determine the optimal geometry of an Al–GMT CMS.

Based on the materials used, the experimental work carried out, and the simulation studies performed, the following conclusions can be drawn:

(1) The mechanical properties of GMTex material are significantly influenced by the number of stacked plies and the woven fabric's orientation. GMTex pressed in two plies shows higher tensile and compressive strengths of 240 MPa and 210 MPa, respectively, compared to 190 MPa and 130 MPa for unpressed GMTex. GMTex in the longitudinal direction of compression molding flow direction exhibits higher tensile and compressive strength compared to the transverse direction.

(2) Using the predeveloped tooling concept, both pure GMTex and an Al–GMT hybrid crash box could be successfully hybrid-formed. The GMTex thickness distribution was homogeneous and thus can be considered satisfactory. However, the fiber filling of GMTex in thin ribs was limited, restricting the design freedom of GMTex.

(3) During axial loading in drop tower tests, pure GMTex crash boxes can enable continuous and progressive failure under axial impact loading through GMTex matrix and fiber failure as well as delamination. The deformation and failure behavior of the hybrid crash box is a superposition of both GMTex and Al materials, which is the folding of Al and crushing of GMTex.

(4) The orthogonal rib configuration (CB3) demonstrated the most favorable balance of high specific energy absorption (*SEA*) and homogeneous force–displacement behavior. The pure GMTex crash box with this kind of optimized structure shows an *SEA* value of 31.4 kJ/kg, compared to ca. 20 kJ/kg for pure aluminum. The Al–GMTex hybrid has a SAE of 32.5 kJ/kg, which is only 3% higher than pure GMTex. However, it prevents any splits of the GMTex materials from escaping the Al profile.

(5) An Al–GMTex hybrid CMS was developed within the current limitations of weldability of the hybrid parts. Without welding limitations, a weight reduction was achieved, however, with consideration of the weldability, the hybrid Al–GMTex CMS was equal to the reference CMS.

(6) The hybrid CMS shows approx. 10% less intrusion and 10% higher mean force level. This could be considered additional weight-saving potential that could not be utilized during this work due to the limitations of minimum aluminum and GMTex rib thicknesses.

A key technological limitation of the present hybrid concept lies in the joining process. Because the aluminum–FRP interface prevents direct welding, hybrid components cannot yet be assembled using conventional technologies. Consequently, additional joining features such as larger flanges, additional C-clamps, mechanical fasteners, or self-piercing rivets are required, adding mass and partially offsetting the lightweight advantage of the hybrid structure. In following investigations, to overcome this limitation, the joining technique between individual hybrid components must be developed such that it enables direct

welding between the hybrid components without flanges and FRP-free zones. Initial work has been conducted by using ultrasonic welding, which should be further investigated.

Author Contributions: Conceptualization, A.H. and X.F.; Methodology, A.H., X.F., S.C.A. and S.J.; Software, S.C.A. and S.J.; Validation, A.H.; Investigation, A.H., X.F., S.C.A. and S.J.; Writing—Original Draft Preparation, A.H. and X.F.; Writing—Review and Editing, X.F. and A.H.; Supervision, X.F.; Project Administration, A.H.; Funding Acquisition, X.F. All authors have read and agreed to the published version of the manuscript.

Funding: This research was funded by the European Regional Development Fund (EFRE), project name: AKTiV (0801129).

Data Availability Statement: All data are contained within the article.

Acknowledgments: The authors would like to thank our project partners Ebmeyer Werkzeugbau GmbH and Martinrea International for their cooperation, as well as the companies Speira GbmH and Evonik AG for their support.

Conflicts of Interest: The authors declare no potential conflicts of interest.

References

1. Jambor, A.; Beyer, M. New cars—New materials. *Mater. Des.* **1997**, *18*, 203–209. [CrossRef]
2. Bisagni, C.; Di Pietro, G.; Fraschini, L.; Terletti, D. Progressive crushing of fiber-reinforced composite structural components of a Formula One racing car. *Compos. Struct.* **2005**, *68*, 491–503. [CrossRef]
3. Fang, X.F. *Karosserieentwicklung und-Leichtbau: Eine Ganzheitliche Betrachtung von Design über Konzept- und Materialauswahlprinzipien bis zur Auslegung und Fertigung*; Springer: Berlin/Heidelberg, Germany, 2023.
4. Ehrenstein, G.W. (Ed.) *Handbuch Kunststoff-Verbindungstechnik*; Hanser: München, Germany, 2004.
5. Messler, R.W. Trends in key joining technologies for the twenty-first century. *Assem. Autom.* **2000**, *20*, 118–128. [CrossRef]
6. Huang, Z.; Sugiyama, S.; Yanagimoto, J. Applicability of adhesive–embossing hybrid joining process to glass-fiber-reinforced plastic and metallic thin sheets. *J. Mater. Process. Technol.* **2014**, *214*, 2018–2028. [CrossRef]
7. Lambiase, F.; Di Ilio, A. Mechanical clinching of metal–polymer joints. *J. Mater. Process. Technol.* **2015**, *215*, 12–19. [CrossRef]
8. Stallmeister, T.; Tröster, T. In-Mold-Assembly of Hybrid Bending Structures by Compression Molding. *Key Eng. Mater.* **2022**, *926*, 1457–1467. [CrossRef]
9. Wang, Z.; Lauter, C.; Sanitther, B.; Camberg, A.; Troester, T. Manufacturing and investigation of steel-CFRP hybrid pillar structures for automotive applications by intrinsic resin transfer moulding technology. *Int. J. Automot. Compos.* **2016**, *2*, 229. [CrossRef]
10. Simacek, P.; Advani, S.G.; Iobst, S.A. Modeling Flow in Compression Resin Transfer Molding for Manufacturing of Complex Lightweight High-Performance Automotive Parts. *J. Compos. Mater.* **2008**, *42*, 2523–2545. [CrossRef]
11. Matsuzaki, R.; Kobayashi, S.; Todoroki, A.; Mizutani, Y. Full-field monitoring of resin flow using an area-sensor array in a VaRTM process. *Compos. Part A Appl. Sci. Manuf.* **2011**, *42*, 550–559. [CrossRef]
12. Hussain, M.M.; Rauscher, B.; Tekkaya, A.E. Wirkmedienbasierte Herstellung hybrider Metall-Kunststoff-Verbundbauteile mit Kunststoffschmelzen als Druckmedium. *Mater. Werkst.* **2008**, *39*, 627–632. [CrossRef]
13. Drossel, W.-G.; Lies, C.; Albert, A.; Haase, R.; Müller, R.; Scholz, P. Process combinations for the manufacturing of metal-plastic hybrid parts. *IOP Conf. Ser. Mater. Sci. Eng.* **2016**, *118*, 012042. [CrossRef]
14. Landgrebe, D.; Kräusel, V.; Rautenstrauch, A.; Albert, A.; Wertheim, R. Energy-efficiency in a Hybrid Process of Sheet Metal Forming and Polymer Injection Moulding. *Procedia CIRP* **2016**, *40*, 109–114. [CrossRef]
15. Wehmeyer, R. *Herstellung von Kunststoff/Metall-Bauteilen Mit Integrierter Umformung im Spritzgießprozess: Production of Plastic/Metal-Hybrid Parts with Integrated Forming in the Injection Moulding Process*; Günter Mainz Verlag: Aachen, Germany, 2012.
16. Hopmann, C.; Schild, J.; Wurzbacher, S.; Tekkaya, A.E.; Hess, S. Combination technology of deep drawing and back-moulding for plastic/metal hybrid components. *J. Polym. Eng.* **2018**, *38*, 583–589. [CrossRef]
17. Fu, S. Effects of fiber length and fiber orientation distributions on the tensile strength of short-fiber-reinforced polymers. *Compos. Sci. Technol.* **1996**, *56*, 1179–1190. [CrossRef]
18. Song, Y.; Gandhi, U.; Sekito, T.; Vaidya, U.K.; Hsu, J.; Yang, A.; Osswald, T. A Novel CAE Method for Compression Molding Simulation of Carbon Fiber-Reinforced Thermoplastic Composite Sheet Materials. *J. Compos. Sci.* **2018**, *2*, 33. [CrossRef]
19. Song, Y.; Gandhi, U.; Pérez, C.; Osswald, T.; Vallury, S.; Yang, A. Method to account for the fiber orientation of the initial charge on the fiber orientation of finished part in compression molding simulation. *Compos. Part A Appl. Sci. Manuf.* **2017**, *100*, 244–254. [CrossRef]

20. Schemme, M. LFT—Development status and perspectives. *Plast. Addit. Compd.* **2008**, *10*, 38–43. [CrossRef]
21. Fang, X.F.; Kloska, T. Hybrid forming of sheet metals with long Fiber-reinforced thermoplastics (LFT) by a combined deep drawing and compression molding process. *Int. J. Mater. Form.* **2020**, *13*, 561–575. [CrossRef]
22. Fang, X.F.; Kloska, T.; Hajdarevic, A. Die Concepts and formability for simultaneous forming of sheet metals and FRPs. *IOP Conf. Ser. Mater. Sci. Eng.* **2022**, *1238*, 012008. [CrossRef]
23. Kloska, T.; Fang, X.F. Lightweight Chassis Components—The Development of a Hybrid Automotive Control Arm from Design to Manufacture. *Int. J. Automot. Technol.* **2021**, *22*, 1245–1255. [CrossRef]
24. Belingardi, G.; Beyene, A.T.; Koricho, E.G.; Martorana, B. Alternative lightweight materials and component manufacturing technologies for vehicle frontal bumper beam. *Compos. Struct.* **2015**, *120*, 483–495. [CrossRef]
25. Moghaddam, A.R.M.; Ahmadian, M.T. Design and Analysis of an Automobile Bumper with the Capacity of Energy Release Using GMT Materials. *World Acad. Sci. Eng. Technol. Int. J. Mech. Aerosp. Ind. Mechatron. Manuf. Eng.* **2011**, *5*, 865–872.
26. Li, Y.; Lin, Z.; Jiang, A.; Chen, G. Experimental study of glass-fiber mat thermoplastic material impact properties and lightweight automobile body analysis. *Mater. Des.* **2004**, *25*, 579–585. [CrossRef]
27. Belingardi, G.; Beyene, A.T.; Jichuan, D. Energy absorbing capability of GMT, GMTex and GMT-UD composite panels for static and dynamic loading—Experimental and numerical study. *Compos. Struct.* **2016**, *143*, 371–387. [CrossRef]
28. Sun, G.; Chen, D.; Zhu, G.; Li, Q. Lightweight hybrid materials and structures for energy absorption: A state-of-the-art review and outlook. *Thin-Walled Struct.* **2022**, *172*, 108760. [CrossRef]
29. Yao, R.; Pang, T.; Zhang, B.; Fang, J.; Li, Q.; Sun, G. On the crashworthiness of thin-walled multi-cell structures and materials: State of the art and prospects. *Thin-Walled Struct.* **2023**, *189*, 110734. [CrossRef]
30. Reuter, C.; Tröster, T. Crashworthiness and numerical simulation of hybrid aluminium-CFRP tubes under axial impact. *Thin-Walled Struct.* **2017**, *117*, 1–9. [CrossRef]
31. Lu, B.; Shen, C.; Zhang, J.; Zheng, D.; Zhang, T. Study on energy absorption performance of variable thickness CFRP/aluminum hybrid square tubes under axial loading. *Compos. Struct.* **2021**, *276*, 114469. [CrossRef]
32. Teimouri, M.; Mahbod, M.; Asgari, M. Topology-optimized hybrid solid-lattice structures for efficient mechanical performance. *Structures* **2021**, *29*, 549–560. [CrossRef]
33. Li, Y.; Qiu, W.; Liu, Z.; Liu, Y.; Xia, L. A multi-material topology optimization approach to hybrid material structures with gradient lattices. *Comput. Methods Appl. Mech. Eng.* **2024**, *425*, 116969. [CrossRef]
34. Rabiee, A.; Ghasemnejad, H. Finite Element Modelling Approach for Progressive Crushing of Composite Tubular Absorbers in LS-DYNA: Review and Findings. *J. Compos. Sci.* **2021**, *6*, 11. [CrossRef]
35. Shi, Y.; Huang, Y.; Morris, Z.; Teoli, M.; Tameer, D.; Kim, I.Y. Stress-Constrained Multi-Material Topology Optimization. *SAE Int. J. Adv. Curr. Prac. Mobil.* **2025**, *7*, 98–111. [CrossRef]
36. Hörmann, M.; Wacker, M. Simulation of the Crash Performance of Crash Boxes based on Advanced Thermoplastic Composite. In Proceedings of the 5th European LS-DYNA User Conference, Birmingham, UK, 25–26 May 2004.
37. Feraboli, P.; Wade, B.; Deleo, F.; Rassaian, M.; Higgins, M.; Byar, A. LS-DYNA MAT54 modeling of the axial crushing of a composite tape sinusoidal specimen. *Compos. Part A Appl. Sci. Manuf.* **2011**, *42*, 1809–1825. [CrossRef]
38. Jayakumar, S.; Hajdarevic, A.; Anand, S.; Fang, X.F. Experimental and FE analyses of the crushing and bending behaviors of GMT and hybrid-formed Al-GMT structures. *Thin-Walled Struct.* **2023**, *186*, 110648. [CrossRef]
39. Hartlen, D.C.; Montesano, J.; Cronin, D.S. Cohesive Zonen Modeling of Adhesively Bonded Interfaces: The Effect of a Adherend Geometry, Element Selection, and Loading Condition. In Proceedings of the 16th International LS-DYNA® Users Conference, Virtual, 10–11 June 2020.
40. *DIN EN ISO 6892-1*; Metallic Materials—Tensile Testing—Part 1: Method of Test at Room Temperature (ISO 6892-1:2019). DIN Deutsches Institut für Normung e.V.: Berlin, Germany, 2019.
41. *DIN EN ISO 527-4*; Plastics—Determination of Tensile Properties—Part 4: Test Conditions for Isotropic and Orthotropic Fibre-Reinforced Plastic Composites (ISO 527-4:2023). DIN Deutsches Institut für Normung e.V.: Berlin, Germany, 2019.
42. *ASTM D 6641/D 6641M*; Standard Test Method for Compressive Properties of Polymer Matrix Composite Materials Using a Combined Loading Compression (CLC) Test Fixture. American Society for Testing and Materials (ASTM): West Conshohocken, PA, USA, 2023.
43. *DIN EN 1465*; Adhesives—Determination of Tensile Lap-Shear Strength of Bonded Assemblies. DIN Deutsches Institut für Normung e.V.: Berlin, Germany, 2009.
44. Kloska, T. *Leichtbaupotenziale im Fahrwerk—Multi-Material-Design Durch Simultane Umformung von Metallblechen und Urformung von Langfaserverstärkten Thermoplasten (LFT)*; Universitätsverlag Siegen: Siegen, Germany, 2020.
45. Jayakumar, S.; Anand, S.; Fang, X. Design Optimization and Validation of GMT Hat Structures. In Proceedings of the 14th International Conference on the Technology of Plasticity—Current Trends in the Technology of Plasticity, Mandelieu-La Napoule, France, 24–29 September 2023; Mocellin, K., Bouchard, P.-O., Bigot, R., Balan, T., Eds.; Springer Nature Switzerland: Cham, Switzerland, 2024; pp. 768–776. [CrossRef]

46. Lau, S.T.W.; Said, M.R.; Yaakob, M.Y. On the effect of geometrical designs and failure modes in composite axial crushing: A literature review. *Compos. Struct.* **2012**, *94*, 803–812. [CrossRef]
47. Striewe, J.; Reuter, C.; Sauerland, K.-H.; Tröster, T. Manufacturing and crashworthiness of fabric-reinforced thermoplastic composites. *Thin-Walled Struct.* **2018**, *123*, 501–508. [CrossRef]
48. Wade, B.; Deleo, F.; Feraboli, P.; Rassaian, M. Crushing of Composite Structures: Experiment and Simulation. In Proceedings of the 50th AIAA/ASME/ASCE/AHS/ASC Structures, Structural Dynamics, and Materials Conference, Palm Springs, CA, USA, 4–7 May 2009; American Institute of Aeronautics and Astronautics: Palm Springs, CA, USA, 2009. [CrossRef]
49. Cheng, P.; Wang, Q.; Ke, S. Energy absorption characteristics of thin-walled steel tube filled with paper scraps. *BioResources* **2021**, *16*, 5985–6002. [CrossRef]
50. Klocke, F.; Schreiner, T.; Schüler, M.; Zeis, M. Material Removal Simulation for Abrasive Water Jet Milling. *Procedia CIRP* **2018**, *68*, 541–546. [CrossRef]
51. Schüler, M.; Heidrich, D.; Herrig, T.; Fang, X.F.; Bergs, T. Automotive hybrid design production and effective end machining by novel abrasive waterjet technique. *Procedia CIRP* **2021**, *101*, 374–377. [CrossRef]

Disclaimer/Publisher's Note: The statements, opinions and data contained in all publications are solely those of the individual author(s) and contributor(s) and not of MDPI and/or the editor(s). MDPI and/or the editor(s) disclaim responsibility for any injury to people or property resulting from any ideas, methods, instructions or products referred to in the content.